RADAR CROSS SECTION REDUCTION OF MICROSTRIP PATCH ANTENNA USING METASURFACES/FRACTALS

Synopsis of the PhD Thesis

Submitted by

Krunal K Patel

(Roll No 70821017007)

Department of Electronics and Telecommunication

Supervisor

Dr. Manjusha Joshi,

Associate Professor, Amity University,
Mumbai

submitted in partial fulfillment of the requirements of

DOCTOR OF PHILOSOPHY (Engineering)

MUKESH PATEL SCHOOL OF TECHNOLOGY MANAGEMENT & ENGINEERING
SVKM's NARSEE MONJEE INSTITUTE OF MANAGEMENT STUDIES (Declared as Deemed-to-be University Under Section 3 of the UGC Act, 1956)
V. L. Mehta Road, Vile Parle (West)
MUMBAI –400056

April 2023

TABLE OF CONTENTS

SECTION NO.	TITLE	PAGE NO.
1	ABSTRACT	1
2	INTRODUCTION	2
3	RESEARCH OBJECTIVES	4
4	LITERATURE REVIEW 4.1 Research Gaps 4.2 Problem Statement	6 7 7
5	CONTRIBUTIONS 5.1 Contribution 1 5.2 Contribution 2 5.3 Contribution 3 5.4 Contribution 4 5.5 Contribution 5	8 8 14 23 35 43
6	Conclusion	49
7	Future Scope	50
8	Publications	51
9	References	52

1. ABSTRACT

Radar Cross Section (RCS) is an essential parameter in Defence Technology. More and more efforts are being taken to reduce the Radar Cross Section of the targets. Antenna is the sole device of communication on the combat platforms and they should be low observable since they significantly contribute to the overall RCS. It is a challenging task to design antennas which exhibit RCS Reduction with no degradation of radiation pattern. The traditional structures like Salisbury Screen, Jaumann Absorbers have large thickness and narrow absorption bandwidth. So, it is desired that low RCS antennas should have planar configuration. Metasurfaces have capability of manipulating the properties of incident wave and they have planar configurations. So, low RCS antennas can be designed using metasurfaces for operation on stealth platforms.

In the present work various types of low RCS antennas are designed using metasurfaces and their RCS reduction performance and radiation patterns characteristics are observed. Other parameters like Reflection Coefficient, Gain in E-plane and H-plane, RCS reduction under oblique incidence and Bistatic Scattering RCS are also obtained. These parameters are simulated in the commercially available simulation tools and they are verified experimentally.

The novel low RCS antennas are designed mainly using Polarization Conversion Metasurfaces and Artificial Magnetic Conductors. They exhibit wide RCS reduction bandwidth with no degradation in antenna radiation pattern and other parameters. The RCS reduction performance of the fabricated antennas is compared with the Reference Patch antennas resonating at the same frequencies. In addition to these, low RCS antennas based on other methods like change in effective parameters, Intersecting Jerusalem Crosses and Strips and combination of CSRR and Fractals are simulated and their comparison is done in terms of RCS reduction bandwidth, E-plane and H-plane radiation patterns, Gain and Design Complexity.

2. INTRODUCTION

Radar Cross Section is an important parameter in defence technology. Radar cross section reduction techniques are widely used for stealth technology. Antenna is the key device of communication on airborne systems. But it is the greatest contributor to the total Radar Cross Section of the stealth platform. Orthodox methods of using Radar Absorbing Materials are used to control the RCS. In addition to this the methods like target shaping and use of active elements for phase cancellation are also prevalent. The use of Radar Absorbing Coating degrades the antenna radiation pattern. In case of airborne systems target shaping is also not of use since aerodynamic shape of the target is also important and a compromise between the shape and Radar Cross Section is inevitable. Recent techniques of RCS reduction use metasurfaces which manipulate the reflection phases of the incident plane wave on the target. Metasurfaces are thin in nature and microstrip antennas can be loaded with metasurface to achieve RCS reduction. The types of metasurface that can be used for RCS reduction include Polarization Conversion Metasurface, Artificial Magnetic Conductors, Complementary Split Ring Resonators and multiband absorbers. Apart from this, fractal geometries and combinations of metasurfaces and fractals are also used to achieve radar cross section reduction.

Periodic structures are used in a variety of applications like Airborne Radomes, Band-Reject Filters, Subreflectors and Main Reflectors with Dichroic Structures, Circuit Analog Absorbers and Meanderline Polarizers. Hybrid Radomes were designed to reduce the out-of-band Radar Cross Section of antennas. With the help of Frequency Selective Surfaces, planar and non-planar antennas are designed to be imperceptible in the direction of backscatter over a wider bandwidth. Antennas mounted on masts can be covered by Frequency Selective Surface to deflect out of band incident plane waves. A dual reflector Cassegrainian system has the hyperboloid made of a dichroic structure which is a periodic structure allows one frequency band and rejects the other frequency band. Periodic structures can be made of lossy material to obtain RCS reduction. Lossy periodic structures are used in Circuit Analog Absorbers. Such periodic structures include crossed elements made of a resistive material. Using meanderline polarizers a tilted wave can be decomposed into two orthogonal components. The resonant frequency of any frequency selective surface can be changed by the addition of dielectric layer below it.

Radar Cross Section can be reduced significantly with the help of Metasurfaces. Metamaterials are artificial structures that have substantial proficiency of manipulating the

properties of the incident electromagnetic wave. They are designed to exhibit unusual Electromagnetic properties like negative permittivity and permeability. The unit cells contain metallic resonators which interact with electromagnetic wave and modify the properties of the incident electromagnetic wave. Metamaterials are built from periodically arranged unit cells. Metamaterials have become a remarkable research area and they are used in the applications like cavity resonators, absorbers, terahertz switches etc. The planar versions of metamaterials are known as metasurfaces and they are designed to manipulate the polarization, the phase, and the amplitude of electromagnetic fields. A rich heterogeneity of metasurface applications has been observed in the literature hitherto.

The present state of the art uses the methods like Radar Absorbing Materials, Frequency Selective Surfaces, Fractal Structures, Superstrates and Resistive Loading. It is required to increase the RCS reduction bandwidth along with proper radiation pattern performance. The research work aims to design Low-RCS antennas and metasurfaces which can provide wide RCS reduction bandwidth for Transverse Electric (TE) as well as Transverse Magnetic (TM) modes. The designed antennas should exhibit wide RCS reduction bandwidth without degradation in antenna radiation pattern and other parameters.

3. RESEARCH OBJECTIVES

Radar Cross Section is a crucial parameter in Defense applications. The Radar Cross Section of air targets like missiles, aircrafts and ground vehicles must be reduced. Antenna is the only device of communication on these platforms. However it is the greatest contributor to the overall RCS. It is required to design Low – RCS antennas to make them imperceptible. The commonly used method of Radar Absorbing Materials exhibit narrowband RCS reduction performance. Apart from this, they degrade the antenna radiation pattern. Traditional metasurfaces, Metamaterial Absorbers and Frequency Selective Surfaces also exhibit narrowband RCS reduction performance. Active elements may be utilized but they increase the design complexity and wideband RCS reduction performance is not assured. Fractal structures can also be used but again their use does not ensure wideband RCS reduction and angular stability.

Microstrip Patch Antennas and their arrays are widely used for communication because of their planar configuration and ease of integration. Metasurfaces also offer the advantages of planar configuration and ease of integration as compared with metamaterials. After analyzing the research gaps, it is required to design Low RCS metasurface based microstrip patch antennas which exhibit wideband RCS reduction for TE as well as TM modes. They should show angularly stable performance. In addition to these, the antenna radiation pattern and other performance parameters should not be degraded.

The research work aims to design novel Low RCS Microstrip Antennas. It also aims to develop novel metasurfaces for wideband RCS reduction. The metasurfaces are designed using Polarization Conversion Metasurfaces (PCMs) and Artificial Magnetic Conductors (AMCs). These methodologies show superior performance as compared with the other methodologies. The unit cells based on PCM structures can be designed and their scattering performance can be analyzed using commercially available simulation tools like CST Microwave Studio and Ansys HFSS. Similarly, AMC unit cells can be analyzed by Periodic Boundary Conditions and their performance under oblique incidence can be studied. New designs of metasurfaces can be investigated which exhibit wideband RCS reduction performance. The designed metasurfaces can be integrated with microstrip patch antenna. It has been observed that the antennas exploiting PCM and AMC based metasurface show wideband RCS reduction performance. The radiation pattern and other performance parameters of these antennas do not degrade if proper optimization is done and angular stability can also be obtained. It is a challenging task to design the antennas which offer wide

RCS reduction bandwidth without degradation of antenna radiation pattern. It is also challenging to enhance the gain of the Low-RCS antennas. The research work utilizes the simulation tools like CST Microwave Studio and Ansys HFSS extensively for proper optimization of the structures.

In addition to these, the research work compares various techniques of RCS reduction with respect to RCS reduction characteristics and other antenna parameters. The comparison helps in finding the most suitable methodologies to satisfy the requirements as per the problem definition. The research work also deals with equivalent circuit modeling of standard shapes like Split Ring Resonator (SRRs), Complementary Split Ring Resonator, Jerusalem Crosses, N-turn SRRs and Spiral Resonators. It also discusses the parameter extraction techniques to obtain the effective parameters like negative permittivity, permeability, refractive index and wave impedance.

4. LITERATURE REVIEW

Due to the excellent properties of metamaterials and metasurfaces, they can be used for various applications like gain enhancement of antennas [1], [2] and Radar Cross Section reduction [3], [4]. Metamaterial absorbers with shielded rear sides have been reported in Ref. [5], [6]. In Ref. [7], MTM absorber was used to achieve RCS reduction, but the device exhibited narrow band performance. The RCS reduction bandwidth was from 7 GHz to 12.8 GHz. The percentage bandwidth was 58.59%.

In Ref. [8], Spiral Coding Metasurface was used to achieve RCS reduction. The metasurface exhibited low RCS reduction bandwidth. It offered percentage bandwidth of 62.92% (13.2 GHz-23 GHz). The surface was not integrated with patch antenna.

In reference [9], Metamaterial Absorber using stacked layer was proposed. The design achieved low RCS reduction bandwidth in the frequency range of 3.15-3.25 GHz. The percentage bandwidth was 3.125%. The design was complex due to stacked layers. S. Genovesi [10] utilized Radar Absorbing Material to reduce RCS, but the use of Radar Absorbing Material degrades the antenna pattern and other parameters. So, it was not suitable for patch antenna. Ref. [11] discusses the stacked layer configuration with MTM absorber. The design was not suitable for a patch antenna. It exhibited absorption bandwidth of 61.33%. Absorption was achieved in the frequency range of 7.8-14.7 GHz. Chen H. [12] proposed the use of radar absorbing material. But the use of Radar Absorbing Material is avoided to maintain antenna performance parameters.

Ref. [13] used fractal structure to achieve RCS reduction. In this paper, the RCS performance was discussed only for the wave incident at 60 deg. RCS reduction was obtained in the frequency range of 2.5-7.5 GHz. In Ref. [14], the use of Radar Absorbing Material was suggested. It caused degradation in antenna radiation performance. The RCS reduction bandwidth was only 9.52% in the frequency range of 6.0-6.6 GHz. Li-Na Chen [15] designed a Minkowski fractal patch antenna for achieving size and Radar Cross Section reduction. The design did not achieve significant RCS reduction over a wide frequency band. The angular stability performance was not discussed properly. It was observed from the results that RCS peaks were reduced but RCS reduction could not be maintained for a wider bandwidth. The RCS performance was discussed only for the angles θ=60 deg., ϕ=0 deg. and θ=60 deg. and ϕ=45 deg. Ref. [16] used 4-bit optimized coding metasurface for achieving RCS reduction. Even though RCS reduction was obtained from 15 GHz to 40 GHz frequency range, the stricture was not suitable for RCS reduction of patch antenna.

4.1) Research Gaps

From the literature survey presented in this section and in the following sections, the following research gaps are observed.

- Conventional metasurfaces and Frequency Selective Surfaces do not exhibit wideband RCS reduction performance
- Metamaterial Absorbers are bandlimited in nature
- Use of Radar Absorbing Materials degrades the antenna radiation pattern
- Target shaping is not useful because of aerodynamic shape of the object
- Conventional metasurfaces and Frequency Selective Surfaces do not show angular stability
- If FSS is exploited, then it may require reflector behind the antenna
- Most of the metasurfaces are not utilized for RCS reduction of patch antennas
- Techniques of Superstrate loading enhance gain but the obtained RCS reduction bandwidth is narrow.
- Superstrate loading also increases the height of the antenna.
- Combination of AMC and PEC (Perfect Electric Conductor) also exhibit narrow RCS reduction bandwidth

4.2) Problem Statement

After analyzing the research gaps, it is essential to design metasurface based Low RCS microstrip patch antennas which provide wide RCS reduction bandwidth for TE as well as TM modes and angularly stable performance without degradation in antenna radiation patterns and other parameters.

5. CONTRIBUTIONS

This section elucidates the original contributions by the researcher. It also discusses as to how the research objectives are attained as per the problem statement.

5.1) Contribution 1: Low-RCS Microstrip Patch Antenna with Polarization Conversion Metasurfcae (Design 1)

In this work, a novel Polarization Conversion Metasurface (PCM) is designed by the author and its RCS reduction characteristics are studied. Then the metasurface is used to design a novel patch antenna which shows RCS reduction over a wide bandwidth. In the published literature, narrowband RCS reduction is observed and the obtained RCS reduction is not significant when the metasurface is integrated with the patch antenna. The main novelty of the proposed design is its wideband RCS reduction performance without degradation in antenna radiation pattern and other parameters and its angular stability.

The PCM structure is designed on an FR-4 substrate with the height of 2.4 mm. The relative permittivity of the substrate is 4.3 and the dielectric loss tangent is 0.02. The conventional SRR geometry is modified to achieve the required polarization conversion as shown in Fig. 5.1.1 (a). In the modified design two additional gaps are created. One split is created in the outer SRR and the other split is created in the inner SRR. Both the splits are located on the opposite sides. The optimized dimensions of the unit cell in mm are as follows: L=7, W=6, t=1, m=0.5, g1=0.5, s=3 and g2=1 mm.

After simulating the unit cell with Periodic Boundary Conditions and Floquet Port Excitation, the resonances and Eigen-modes are found and various configurations of the Polarization Conversion Metasurface are examined. After observing the simulation results, it was found that if the unit cells are arranged in the mirror configuration, then significant RCS reduction is obtained. Fig. 5.1.1 (b) shows the designed metasurface and Fig. 5.1.1 (c) shows the proposed Patch Antenna with PCM. Using the concept of polarization conversion, various configurations of the microstrip patch antennas are examined using the designed metasurface and the configuration which gives the superior RCS reduction performance was selected for the low RCS antenna. The square patch has dimensions of 18 mm × 18 mm and the substrate height is 2.4 mm. The Copper thickness is 35 microns. The ground plane and the substrate dimensions are 70 mm × 70 mm.

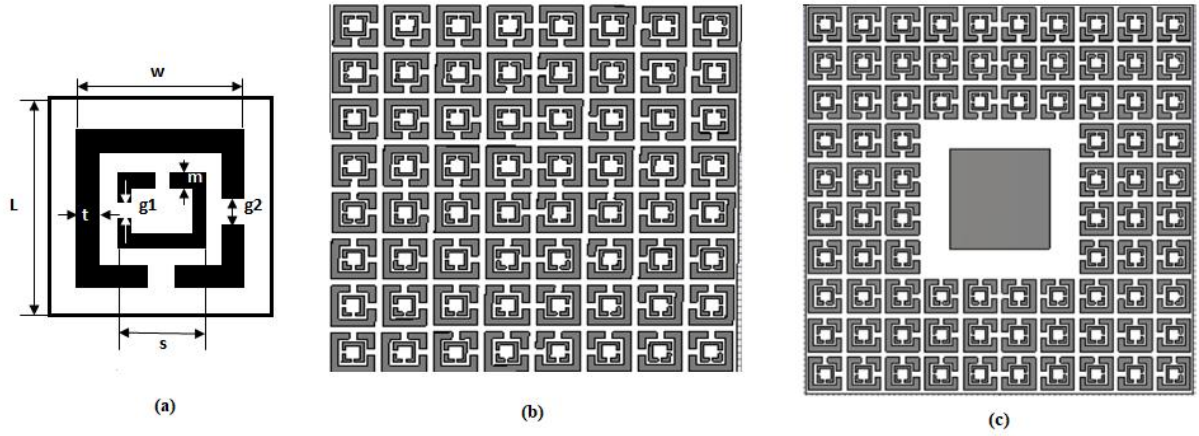

Figure 5.1.1. (a) Modified SRR Geometry, (b) Designed Polarization Conversion Metasurface, (c) Patch Antenna with PCM (Proposed Design)

Configurations 1 to Configuration 4 use less number of unit cells. In Configuration 5 (Proposed Design), more unit cells are added and the unit cells are kept in the mirror configuration. In Configuration 6, all the unit cells of Configuration 5 were rotated by 180 deg.

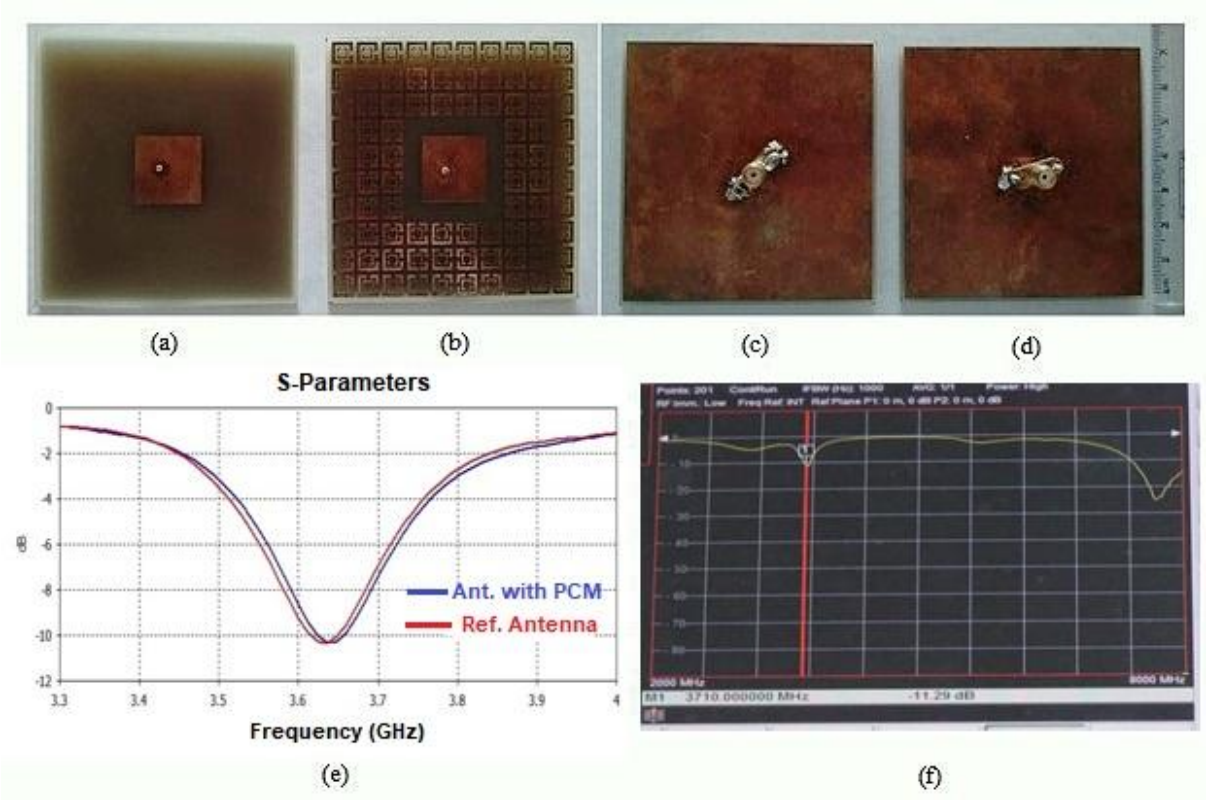

Figure 5.1.2. Fabricated Patch Antennas; (a) Top view of Simple Patch, (b) Top view of Metasurface loaded Patch Antenna, (c) Bottom view of Simple Patch, (d) Bottom view of Metasurface loaded patch antenna, (e) Simulated Reflection coefficients of the Reference Patch and the Antenna with PCM, (f) Experimentally Measured Reflection Coefficient of the Patch Antenna with PCM

The reference patch antenna and the metasurface loaded microstrip patch antenna are simulated in CST Microwave Studio software. The resonant frequency of the conventional

antenna is 3.63 GHz. The modified antenna is resonating at the frequency of 3.6359 GHz which is almost the same as that of the conventional patch antenna.

The top views of the fabricated antennas are shown in Fig. 5.1.2 (a) and Fig. 5.1.2 (b). The bottom views of the fabricated antennas are shown in Fig. 5.1.2 (c) and Fig. 5.1.2 (d). Fig. 5.1.2 (e) shows the simulated reflection coefficients of the Reference Patch Antenna and the Antenna with PCM. Fig. 5.1.2 (f) shows the experimentally measured reflection coefficient of the Antenna with PCM. The simulated reflection coefficient obtained is around -10.31 dB whereas the experimentally measured reflection coefficient is around -11.2 dB.

Fig. 5.1.3 compares the simulated RCS values of the proposed patch antenna, the reference patch antenna and the metal sheet of the same dimensions (70 mm × 70 mm) for TE as well as TM modes. With the proposed patch antenna, overall RCS reduction bandwidth of 3.49 GHz – 20 GHz (140.57%) can be obtained as compared with the metal sheet. At the frequency of 4.66 GHz and from 12 GHz – 14 GHz, RCS reduction is not significant but these short intervals can be neglected as far as theoretical RCS reduction bandwidth is considered. In addition to this, 10 dB RCS reduction is obtained from 8.84 GHz - 10.45 GHz (16.41%) and from 16.99 GHz - 17.81 GHz (4.71%) as compared with the metal sheet. If the proposed antenna is compared with the conventional antenna then overall RCS reduction is obtained from 4.2196 GHz - 11.554 GHz (93%) and from 14.431 GHz - 19.647 GHz (30.61%). 10 dB RCS reduction is obtained from 8.835 GHz to 10.35 GHz (15.79%) and from 17.15 GHz to 17.75 GHz (3.44%). The RCS reduction peaks are observed at 5.46 GHz, 9.1 GHz, 9.89 GHz and 17.41 GHz as shown in the simulation results.

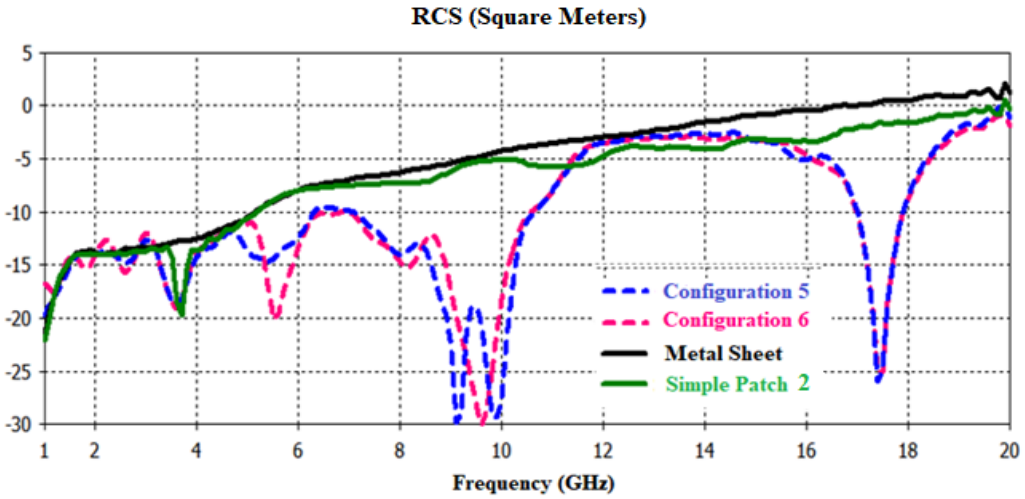

Figure 5.1.3. Simulated Radar Cross Section of the Metal Sheet, Reference Patch and the Antenna with PCM (Configuration 5), (TE, TM) Modes

Fig. 5.1.4 compares experimentally measured RCS values of a metal plate of the same dimensions, patch antenna without metasurface and patch antenna with metasurface. It shows that the RCS values of the metal plate continuously increase with increasing frequency.

If the conventional antenna is used, then it provides almost the same RCS values as those obtained by the metal plate. The patch antenna with metasurface provides significant RCS reduction. The metasurface loaded patch antenna provides RCS reduction peaks at 5.6 GHz, 9.1 GHz and 10.25 GHz frequency points. The RCS values at these frequencies are -18 dBsm, -37 dBsm and -38 dBsm respectively. The overall RCS reduction bandwidth is 4.7 GHz – 11 GHz and 14.5 – 20 GHz as compared with the Reference Patch Antenna. The 10 dB RCS reduction is obtained from 8.8 GHz - 10.65 GHz. RCS reduction of the order of -10 dB is observed from 17.4 GHz - 17.814 GHz.

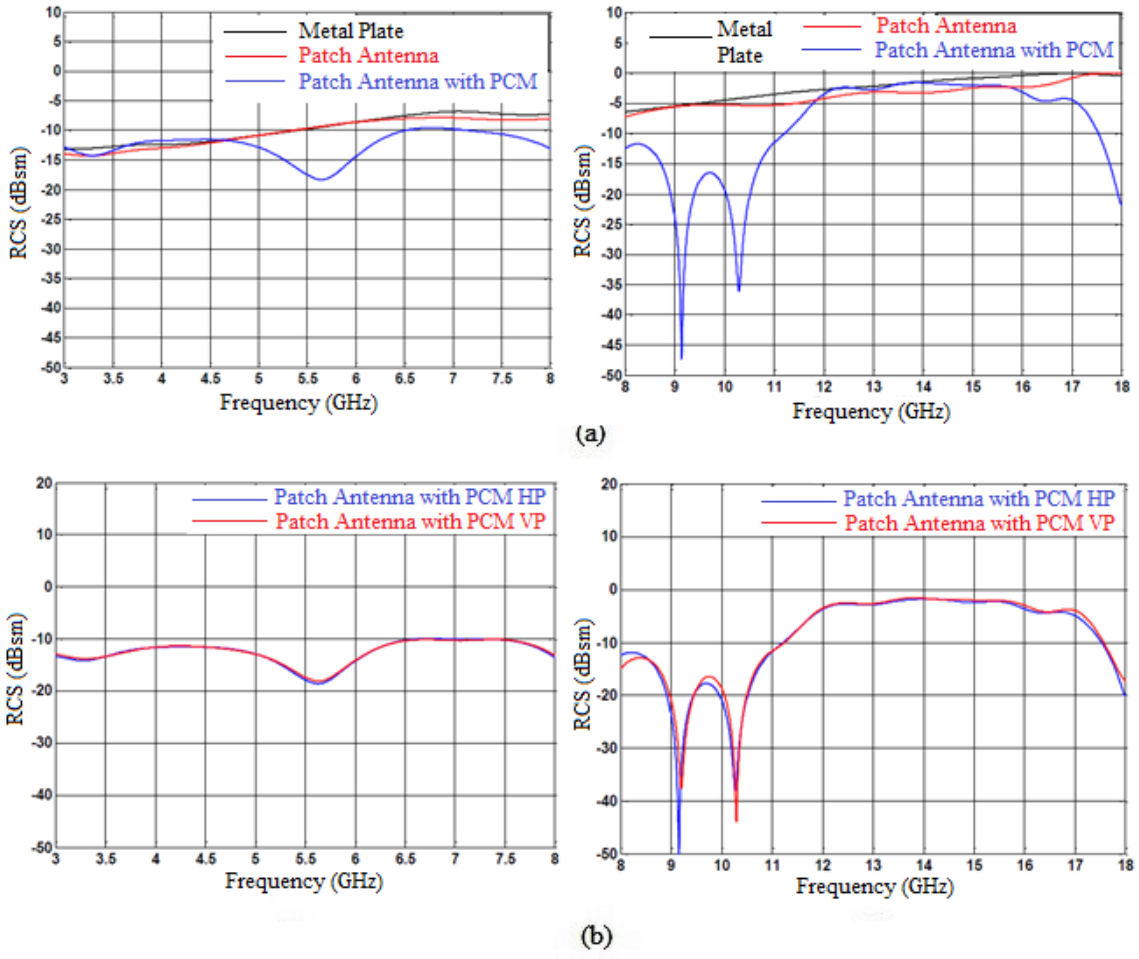

Figure 5.1.4. (a) Experimentally Measured Values of Radar Cross Section from 3 GHz – 18 GHz, (b) Experimentally measured RCS versus frequency response in HP and VP of patch antenna with metasurface from 3 GHz – 18 GHz

Fig. 5.1.5 shows the simulated RCS of the modified antenna for oblique incidence. The RCS values are evaluated at 0 deg., 10 deg. and 20 deg. angles of incidence for the

Transverse Electric mode as well as the Transverse Magnetic mode. Because of the structural symmetry of the antenna, these values remain identical for TE mode as well as TM mode at the normal incidence. The simulated results show that in the case of oblique incidence, better RCS reduction is achieved.

Fig. 5.1.6 (a) and Fig. 5.1.7 (b) show the simulated gain patterns of the conventional patch antenna in both the principal planes. At the resonance frequency, the peak gain value is 4.36 dB in the E-plane. Whereas, the peak gain value is 4.27 dB in the H-plane. Fig. 5.1.6 (c) and Fig. 5.1.6 (d) show the simulated gain patterns of the patch antenna with metasurface in both the principal planes. It shows that the modified antenna has the peak gain value of 4.13 dB in the E-plane. The modified antenna shows the peak gain value of 4.02 dB in the H-plane. After observing the radiation diagrams of both the conventional antenna and the antenna with metasurface, it can be concluded that the metasurface loading does not degrade the antenna radiation parameters. The metasurface reduces the RCS of the antenna significantly.

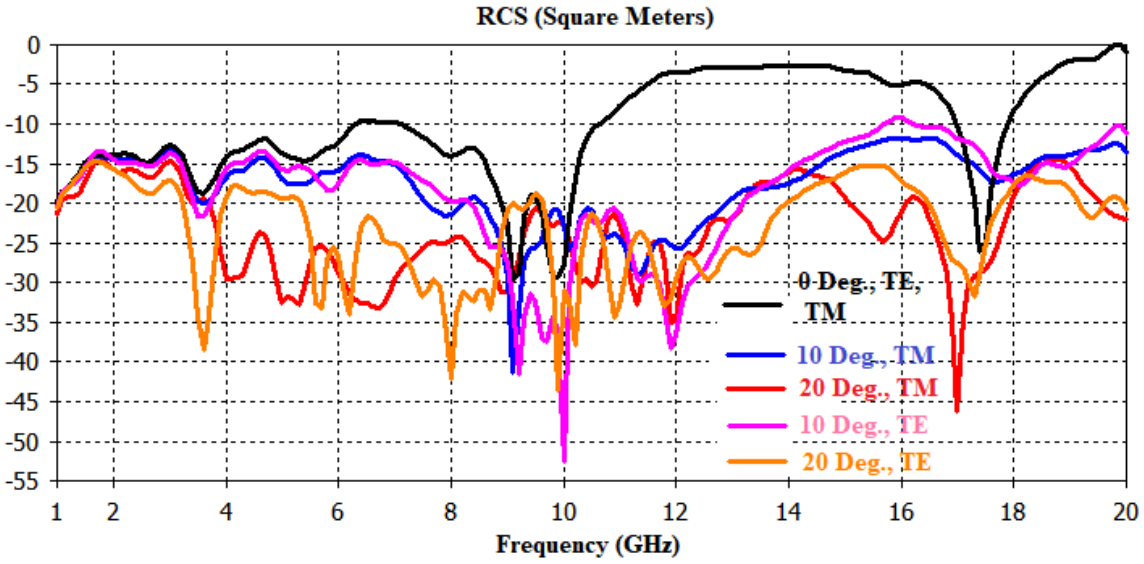

Figure 5.1.5. Simulated RCS of the antenna with PCM at oblique incidence for TE and TM modes

Fig. 5.1.6 (e) and Fig. 5.1.6 (f) show the experimentally measured radiation patterns of the Reference Antenna in both the principal planes. Whereas Fig. 5.1.6 (g) and Fig. 5.1.6 (h) show the measured radiation patterns of the Patch Antenna with Metasurface in both the principal planes. In experimental polar patterns, the main lobe is shown at 90 deg. due to the post-processing of the measurement software data. The experimental polar patterns are plotted from -90 deg. to +90 deg. because of the limitations of the positioner. The experimental results are in a good agreement with the simulated results. The measured gain values in the boresight direction for the Reference Antenna are 3.9 dB in the E-plane and 3.85

dB in the H-plane. The measured gain values for the antenna with PCM are 4.1 dB and 3.55 dB in the E-plane and in the H-plane respectively. The gain is measured by the Friss-Transmission Method.

The proposed design of the patch antenna shows excellent RCS reduction for a wide frequency range and it can be used on the low observable platforms. The simulated and measured results show that excellent out-of-band RCS reduction is obtained without degradation of the antenna radiation pattern. It also shows excellent angular stability up to 70 deg. angle of incidence and RCS reduction is obtained for oblique incidence also. The Polarization Converter Metasurface shows superior performance as compared with Radar Absorbing Materials, Metamaterial Absorbers and other types of Frequency Selective Surfaces. With the help of the proposed design Bistatic RCS reduction can also be achieved.

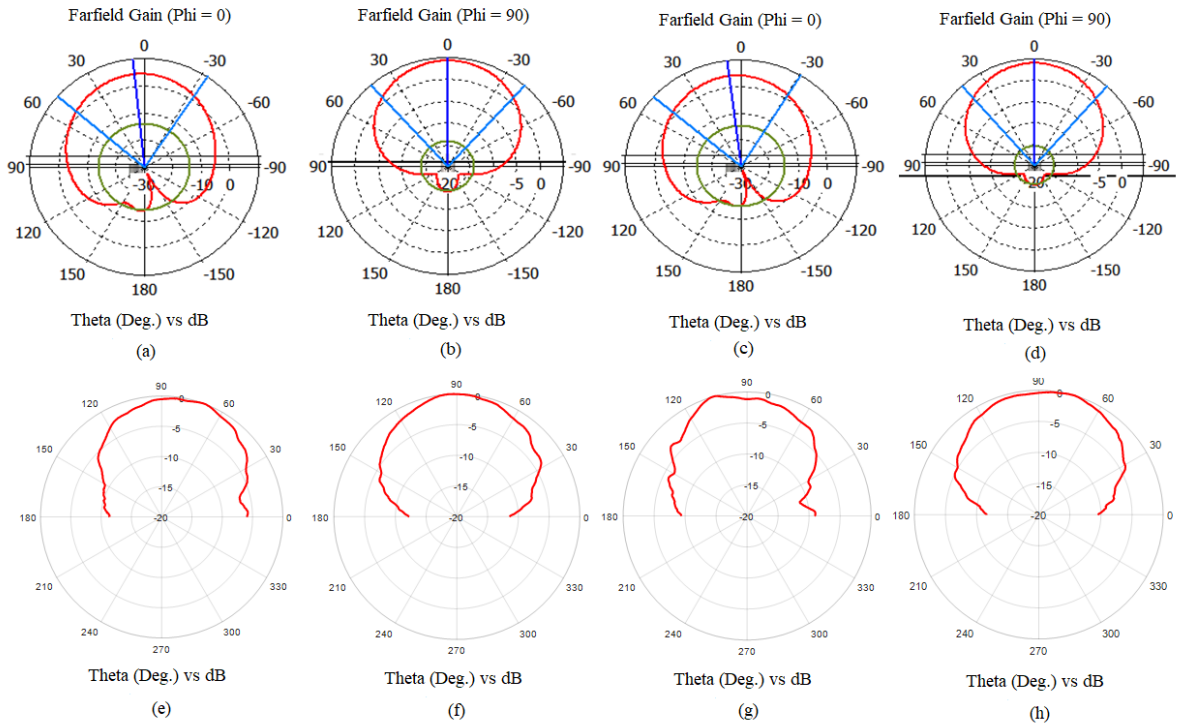

Figure 5.1.6. Simulated Gain patterns of the conventional antenna in (a) E-plane and (b) H-plane; Simulated Gain patterns of the patch antenna with metasurface in (c) E-plane and (d) H-plane; Experimentally Measured Radiation Patterns of the conventional antenna in (e) ϕ = 0 deg. plane and (f) ϕ = 90 deg. plane, Experimentally Measured Radiation patterns of the antenna with metasurface in (g) ϕ= 0 deg. plane and (h) ϕ = 90 deg. plane

Table 5.1.1 shows the comparison of the proposed design with the published work and shows its advantages over the existing state-of-the-art. The comparison is made in terms of RCS Reduction Bandwidth, Design Methodology, Angular Stability, Radiation Pattern Degradation and Design Complexity. The comparison shows that the proposed design offers larger bandwidth for out-of-band RCS reduction, angular stability and no radiation pattern degradation as compared with other methodologies.

Table 5.1.1. Comparison of the proposed design with similar work

Reference, Year of Publication	Methodology Used	Limitations	Percentage Bandwidth	Design Complexity
[17], 2021	Polarization Converter Metasurface	Narrow Bandwidth, Angular stability was not discussed	15.5 GHz – 16.5 GHz (Linear to linear polarization conversion freq. range)	Not used for RCS reduction of antennas
[18], 2019	JC structure based on SRR	Narrow Bandwidth	absorption peaks at 8.6, 10.2, 11.95 GHz	Not integrated with patch
[19], 2016	CSRR	No angular stability, Narrow bandwidth	RCS reduction peaks at 2.2 GHz and at 3.05 GHz	CSRRs in the ground plane
[20], 2016	Polarization Rotator	Not used for RCS reduction of a microstrip antenna	47.75 % (5.50-8.94 GHz) and 16.78 % (13.30-15.50 GHz)	Simple and feasible design
[21], 2013	Polarization Converters	No Polarization conversion for oblique incidence, Narrow BW	2-3.5 GHz (54.55%) (for Conversion Efficiency greater than 56%)	Not integrated with patch
Proposed Design	Polarization Converters	Excellent Angular Stability w.r.t various angles of incidence and polarization (TE as well as TM)	Overall RCS reduction BW [almost 3.49 – 20 GHz (140.57%) as compared with PEC], [4.2196 – 11.554 GHz (93%) and 14.431 – 19.647 GHz (30.61%) as compared with patch]	Single Layer Design, Co-planar integration of metasurface

5.2) Contribution 2: Low-RCS Microstrip Patch Antenna with Polarization Conversion Metasurfcae (Design 2)

In this work, a novel Polarization Conversion Metasurface is proposed and it is integrated with the patch antenna. The metasurface is designed by turning the metallic strip structure by 45 Deg. The RCS reduction performance of the designed antenna is analyzed for TE as well as TM modes. With this novel design, the RCS of the patch antenna can be reduced significantly with an enhancement in radiation pattern characteristics. Wideband RCS reduction can be achieved for parallel as well as perpendicular polarization.

Fig. 5.2.1 (a) shows the design of metasurface unit cell. The length and the width of the metallic strip are ls=6.8 mm and ws=1.5 mm respectively. The length and breadth of the unit cell are l=7 mm and w=7 mm respectively. Fig. 5.2.1 (b) shows the mechanism of polarization conversion. It shows that the incident wave is decomposed into two orthogonal components. One component is the u-polarized wave and the other is the v-polarized wave. It also shows the mechanism of polarization conversion. Ei is the incident Electric Field and Er is the reflected Electric Field.

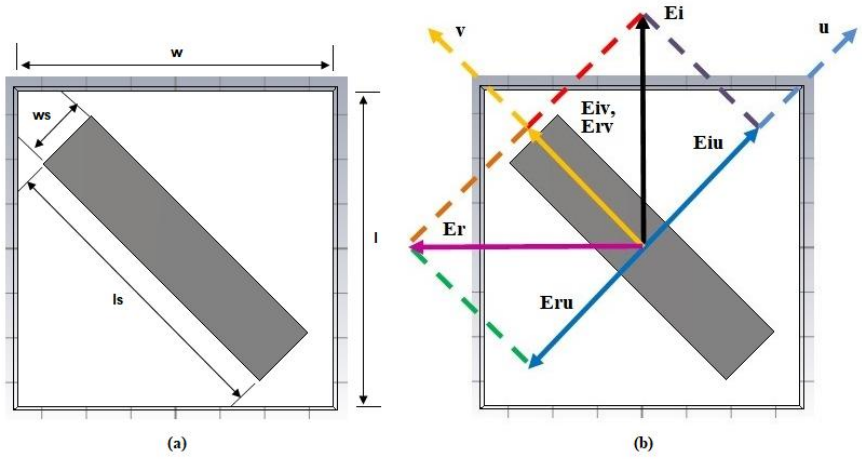

Figure 5.2.1. (a) Design of the unit cell, (b) Mechanism of polarization conversion

To design a low RCS microstrip patch antenna, co-planar integration of the metasurface with the patch antenna is carried out. The antenna is considered perfectly matched with the feed line impedance facilitating the observation of the structural mode RCS of the antenna. Fig. 5.2.2 (a) shows the designed Polarization Conversion Metasurface. Fig. 5.2.2 (b) shows the geometry of the Microstrip Patch Antenna with Polarization Converter Metasurface. The low-RCS antenna is designed on the same FR-4 substrate having thickness (h) of 2.4 mm, dielectric constant (ε_r) of 4.3 and loss-tangent (tanδ) of 0.02. The square patch antenna has dimensions of 8 mm × 8 mm. The length and width of the ground plane and the substrate are l_g=70 mm and w_g=70 mm respectively. The Cu thickness is 0.035 mm. The low RCS antenna uses an array of 10 × 10 unit cells for coplanar integration with the patch antenna. Fig. 5.2.3 shows the top and bottom views of the fabricated microstrip patch antennas. They are fabricated using the standard PCB fabrication technology.

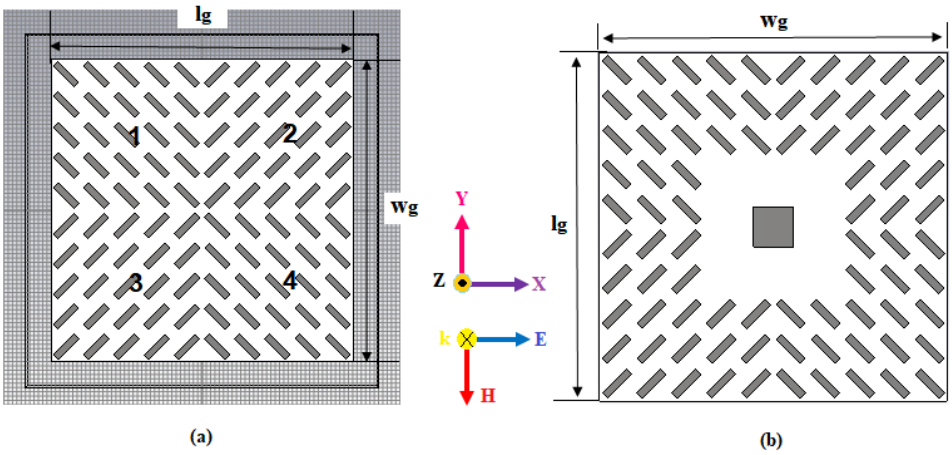

Figure 5.2.2. (a) Design of the Polarization Converter Metasurface for RCS reduction (b) Microstrip Patch Antenna with PCM

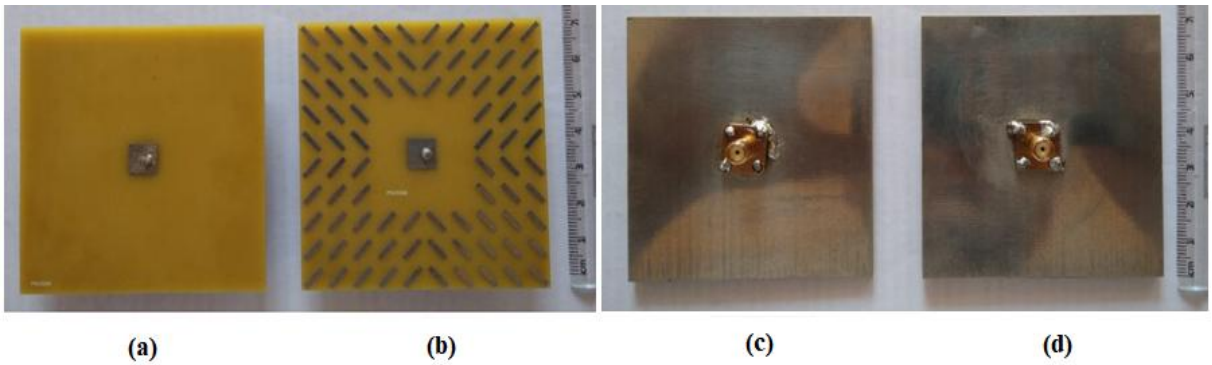

Figure 5.2.3. Top view of fabricated antennas (a) Ref. Patch, (b) Antenna with PCM; Bottom view of fabricated antennas (c) Ref. Patch, (d) Antenna with PCM

The Reference Antenna and the Low RCS Antenna are simulated in CST Microwave Studio software. Fig. 5.2.4 shows the simulated RCS of the metal plate, the Reference Antenna and the Antenna with PCM.

From simulation results, it is observed that, the overall RCS reduction bandwidth of 7.25 GHz – 24.83 (110 %) GHz is obtained as compared with the metal sheet and the Reference Patch antenna. 10 dB RCS reduction is obtained from 8.33 GHz – 9.16 GHz (9.49 %) and from 12.81 GHz – 18.85 GHz (38.16 %) as compared with the Reference Patch antenna. The RCS reduction peaks are observed at 8.9 GHz in the X-band and at 14.52 GHz in the Ku-band. The RCS values are -32.17 dBsm and -29.91 dBsm at these frequencies respectively.

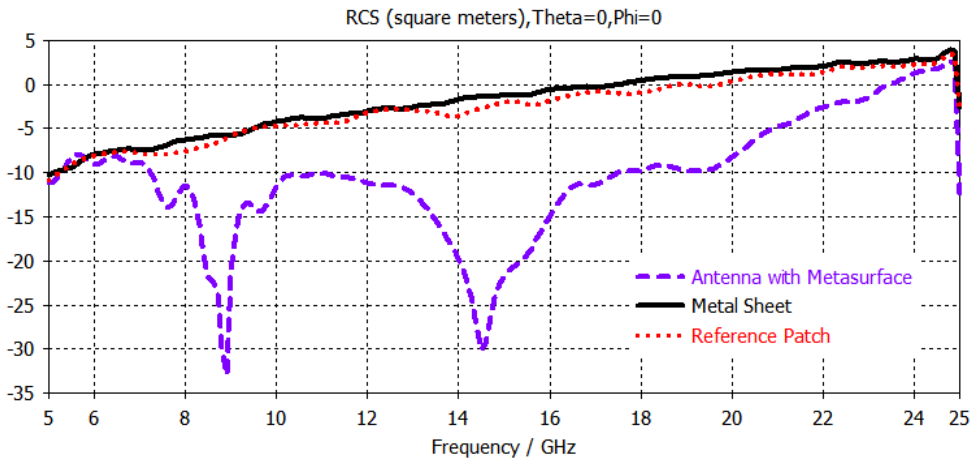

Figure 5.2.4. Simulated values of RCS (TE, TM modes)

Fig. 5.2.5 (a) shows the experimentally measured RCS values of the Metal Plate, the Reference Patch and the Antenna with PCM for the TE mode. The results show that the Antenna with PCM shows an RCS reduction peak at 9.41 GHz in X-band and the measured RCS value is -23.34 dBsm at this frequency. The design shows another RCS reduction peak at 14.745 GHz in Ku-band and the measured RCS value is -37.66 dBsm. Whereas, 10 dB RCS reduction bandwidth of 13.3% and 35.38% is obtained in the X-band and the Ku-band respectively. The simulated and experimentally measured results are in well agreement. Fig. 5.2.5 (b) shows the experimentally measured RCS values of the Metal Plate, the Reference Patch and the Antenna with PCM for the TM mode.

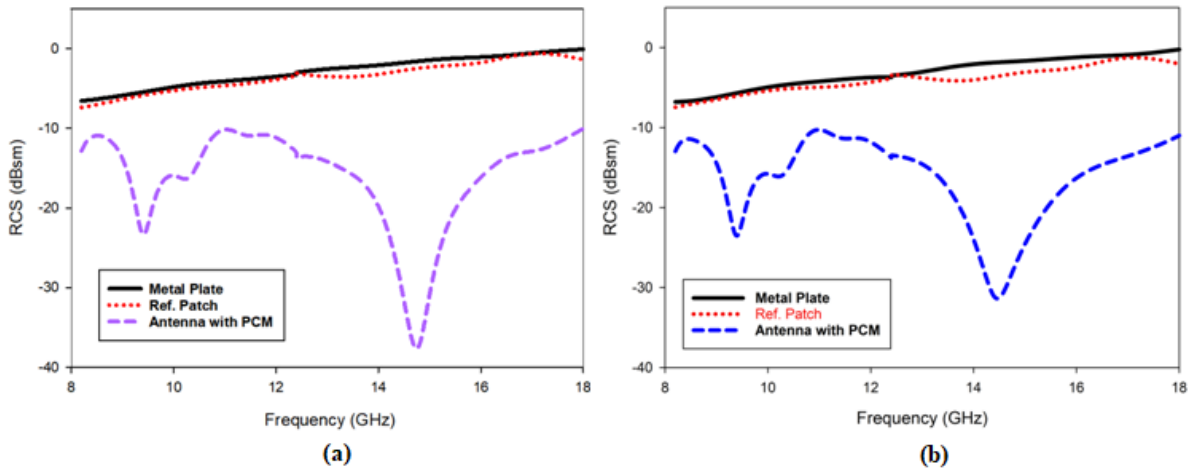

Figure 5.2.5. (a) Experimentally measured values of RCS (TE Mode), (b) Experimentally measured values of RCS (TM Mode)

Fig. 5.2.6 shows the RCS characteristics of the Antenna with PCM under oblique incidences for the Transverse Electric mode. Fig. 5.2.7 shows the RCS characteristics of the Antenna with PCM under oblique incidences for the Transverse Magnetic mode. It is inferred from the figures that the antenna shows good RCS reduction for angles of incidence

upto 30 deg. If the angle of incidence is increased, then also RCS reduction is observed with some shifts in peak RCS reduction frequencies.

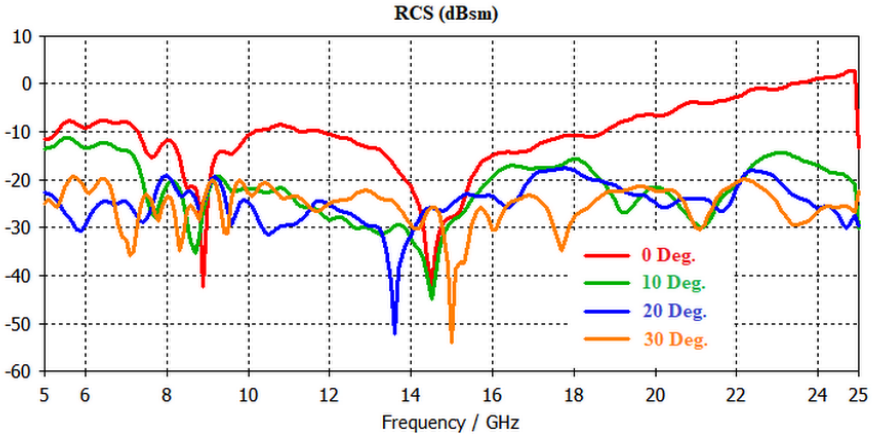

Figure 5.2.6. RCS of the Antenna with PCM under oblique incidence (TE Mode)

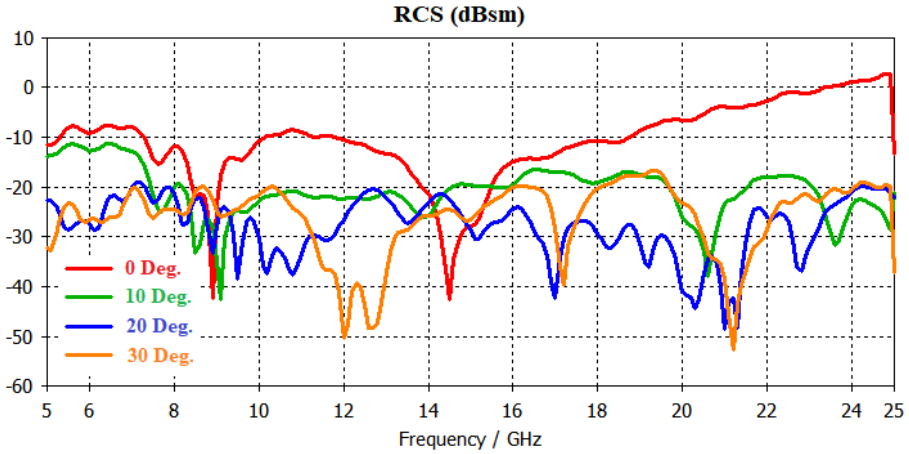

Figure 5.2.7. RCS of the Antenna with PCM under oblique incidence (TM Mode)

Fig. 5.2.8 (a) shows the simulated reflection coefficients of the Reference Antenna and the Antenna with PCM structures. Fig. 5.2.8 (b) shows the experimentally measured Reflection Coefficient of the Antenna with PCM. The resonant frequency of the simple patch antenna is 7.535 GHz as shown in the simulation results. The value of Reflection Coefficient is around -17.5 dB. The simulated Reflection Coefficient of the Antenna with PCM is around -17 dB at the resonant frequency of 7.5483 GHz. The experimentally measured Reflection Coefficient of the Antenna with PCM is around -13.5 dB at the resonant frequency of 7.31 GHz. There is a good agreement between the simulated and experimentally measured results.

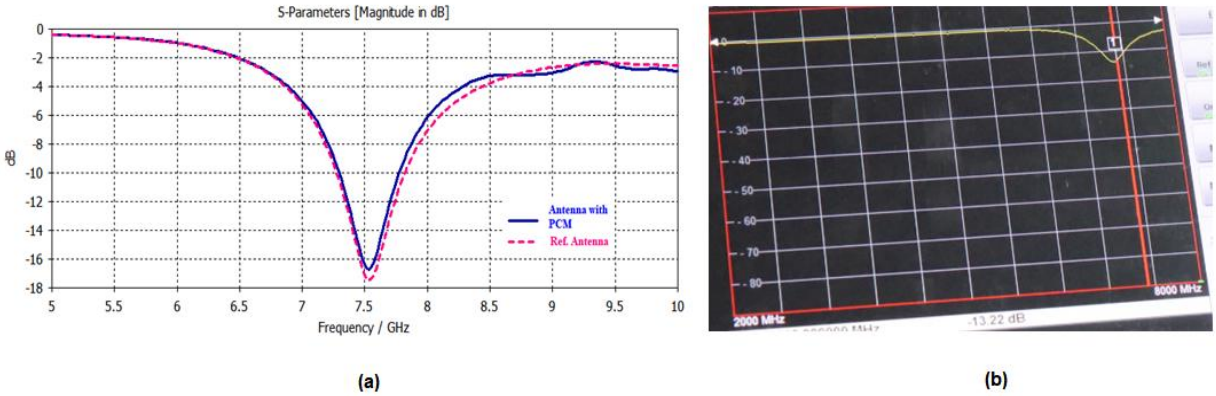

Figure 5.2.8. (a) Simulated Reflection Coefficients of the Ref. Antenna (Dashed) and the Antenna with PCM (Solid) (b) Experimentally measured Reflection Coefficient of the Antenna with PCM

Fig. 5.2.9 shows the simulated Gain patterns in the ϕ= 0 deg. plane and the ϕ=90 deg. plane. For the Reference Antenna, the gain value is 2.385 dB in the boresight direction of the E-plane and the peak gain value is 5.65 dB. The value of gain in the H-plane is 2.36 dB. For the Antenna with PCM, the main lobe is directed at 0 deg. in the E-plane and in the H-plane. The peak gain value is 5.81 dB in the ϕ=0 deg. plane and in the ϕ=90 deg. plane. So, as compared with the Reference antenna the radiation pattern of the Antenna with PCM improves since it is directed at 0 deg. in both the planes. The gain enhancement in the H-plane results from the slight mutual coupling of the metasurface elements and patch.

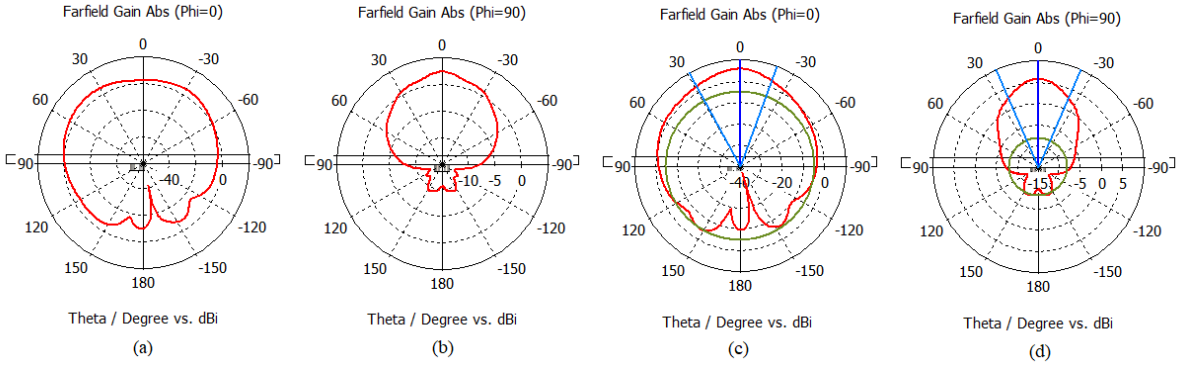

Figure 5.2.9. Simulated Far-field Gain patterns of the Reference Antenna (a) ϕ=0 Deg. plane (b) ϕ=90 Deg. plane, Simulated Far-field Gain patterns of the Antenna with PCM (c) ϕ=0 Deg. plane (d) ϕ=90 Deg. plane

Fig. 5.2.10 shows the experimentally measured radiation patterns of the Reference Antenna and the Antenna with PCM in the ϕ=0 deg. plane and in the ϕ=90 deg. plane. The Friis-Transmission method is used to calculate the gain of the antennas. The measured Gain value of the Reference Antenna is 2.87 dB in the boresight direction of the E-plane and 3.78 dB in the H-plane. The measured Gain values of the antenna with PCM are 5.97 dB in the E-plane and 5.79 dB in the H-plane.

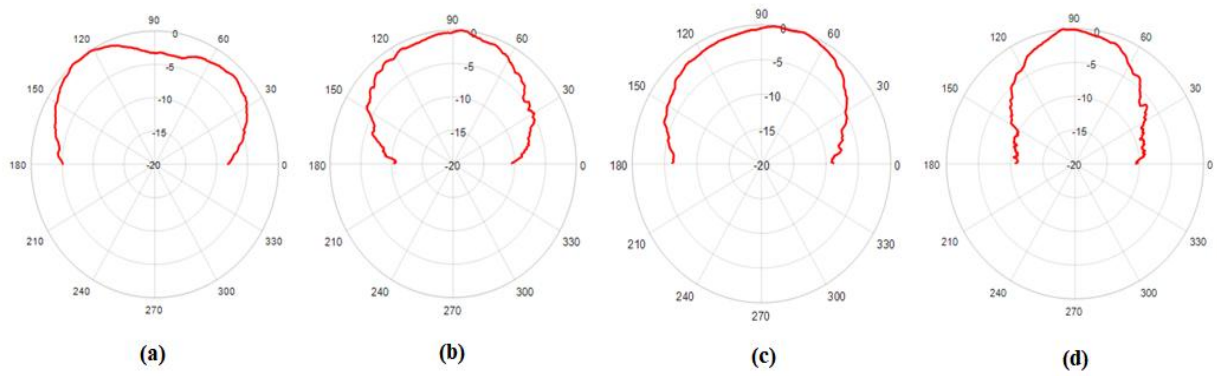

Figure 5.2.10. Experimentally measured Far-field radiation patterns of the Reference Antenna (a) ϕ=0 Deg. plane (b) ϕ=90 Deg. plane, Experimentally measured Far-field radiation patterns of the Patch Antenna with metasurface in (c) ϕ=0 Deg. plane (d) ϕ=90 Deg. plane

The experimentally measured values are almost the same as those obtained by the simulation. Slight differences may be observed due to fabrication tolerances and line losses. In the experimental polar patterns, the main lobe is directed at 90 deg. due to the post-processing of the measurement data in the software. The experimental polar patterns are plotted from -90 deg. to +90 deg. since the positioner could not be rotated beyond 90 deg. due to the supporting structure.

Fig. 5.2.11 shows the bistatic scattering at 9.1037 GHz frequency. The RCS values of the Metal Sheet, the Reference Patch and the Antenna with PCM are -5 dBsm, -5.1 dBsm and -17.6 dBsm respectively in the phi=0 deg. plane. It shows RCS reduction of 12.6 dBsm and 12.5 dBsm as compared with the metal sheet and the reference patch.

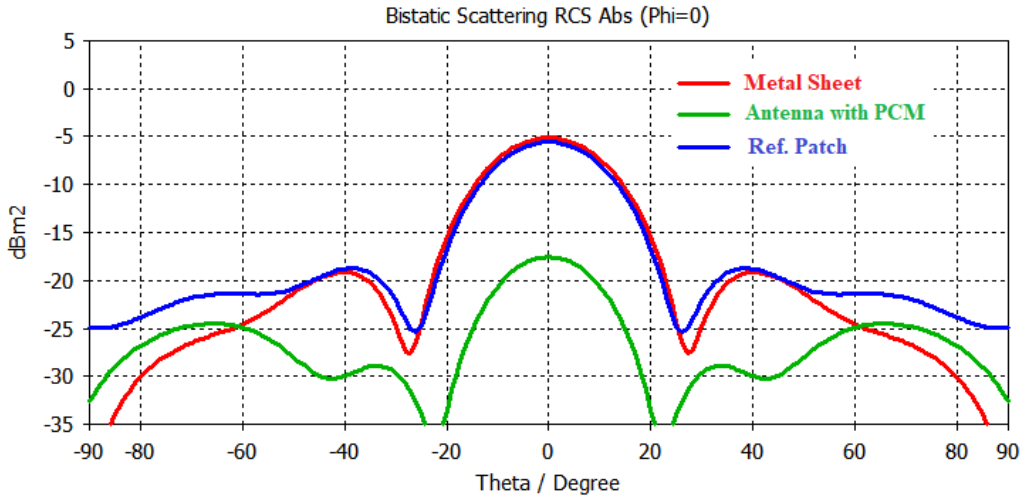

Figure 5.2.11. Bistatic scattering at 9.1037 GHz

Fig. 5.2.12 shows the bistatic scattering RCS at 13.655 GHz frequency. The RCS values of the Metal Sheet, the Reference Patch and the Antenna with PCM are -1.89 dBsm, -3.42 dBsm and -17.84 dBsm respectively in the phi=0 deg. plane. It shows RCS reduction of 15.95 dBsm and 14.42 dBsm as compared with the Metal Sheet and the Reference Patch

respectively at this frequency. Significant RCS reduction is observed for a wide angular range. Bistatic RCS reduction can also be observed at the other resonance frequencies of Polarization Conversion Metasurface.

Fig. 5.2.13 shows the 3D scattering comparison of the Metal Sheet, Reference Patch Antenna and the Antenna with PCM at the frequency of 9.1037 GHz. In the cases of Metal Sheet and Reference Patch Antenna, the reflected beam maxima are directed at 0 deg. For the Antenna with PCM, the reflected beam is scattered in various directions and the reflection is minimized in the boresight direction. So, RCS reduction mechanism can also be explained with the help of 3D scattering patterns.

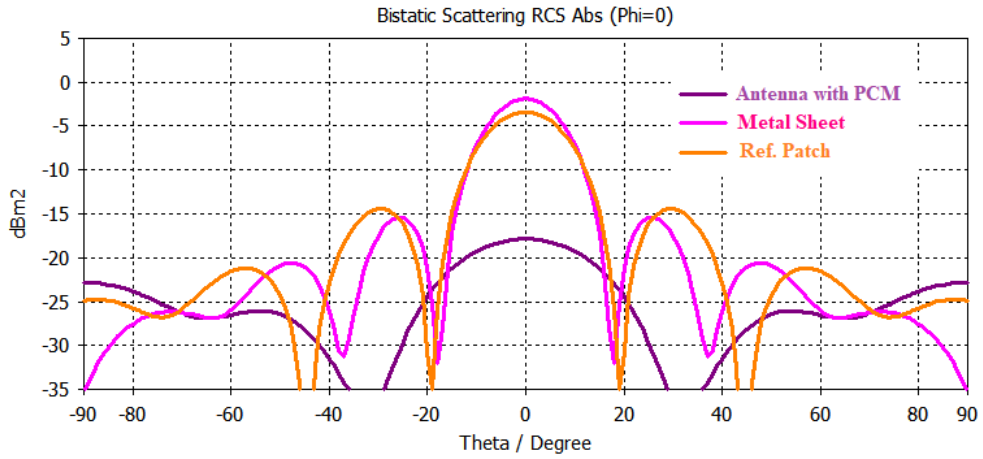

Figure 5.2.12. Bistatic scattering at 13.655 GHz

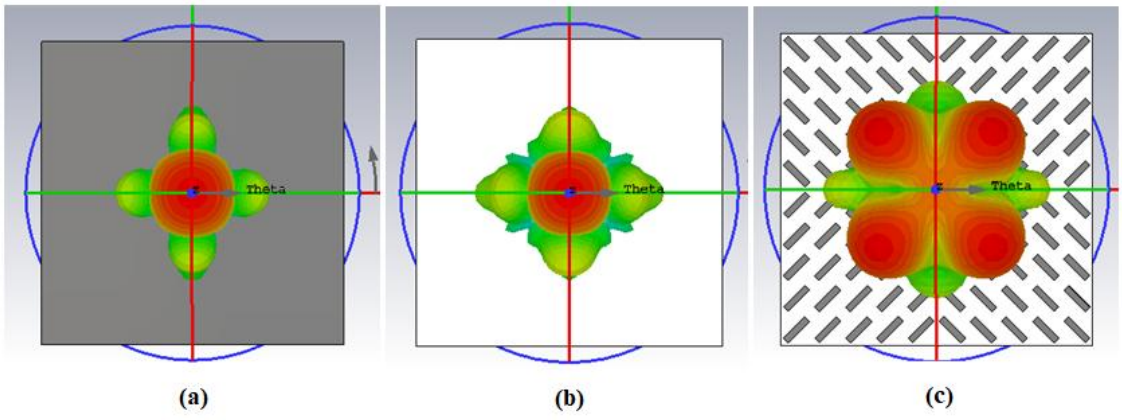

Figure 5.2.13. 3D scattering at the frequency of 9.1037 GHz (a) Metal Sheet, (b) Reference Patch Antenna, (c) Antenna with PCM

Table 5.2.1 shows the advantages of the proposed design over the present state-of-the-art. The comparison is done in terms of percentage bandwidth of RCS reduction, radiation pattern characteristics, methodology used and design complexity. It is observed from the comparison that most of the designs suffered from narrow bandwidth. Recently developed metasurfaces are not used to reduce the RCS of the patch antenna. From the simulation and

experimental results, it can be inferred that for the patch antenna with PCM, no degradation of Radiation Pattern and Gain is observed. Excellent Radar Cross Section reduction is obtained for the Transverse Electric as well as the Transverse Magnetic mode. Significant RCS reduction can also be observed in the cases of oblique incidences. With this design, Monostatic as well as Bistatic RCS reduction can be obtained.

Table 5.2.1. Comparison of the proposed design using PCM with similar work

Ref. , Year of Publication	**Methodology Used**	**Features**	**Percentage Bandwidth**	**Design Complexity**
[17], 2021	Polarization Converter Metasurface	Narrow BW, No discussion of Angular Stability	15.5 GHz – 16.5 GHz (For linear to linear polarization conversion)	Not used for RCS reduction of patch antennas
[18], 2019	Jerusalem Cross based on Split Ring Resonator	Narrow Bandwidth	absorption peaks observed at 8.6, 10.2, 11.95 GHz	Not integrated with microstrip antenna
[22], 2018	Circular Ring with Parasitic Cross- AMC	Narrow Bandwidth	8.2-10.25 GHz (22.22%)	Not used for RCS reduction of antennas
[23], 2019	Optimized Coding Metasurface (AMC)	Narrow Bandwidth, No RCS reduction in the X-Band	12.2-19.8 GHz (48%)(> 7 dB RCS reduction BW)	Co-planar integration of the metasurface with the patch antenna
[24], 2017	Pixelated Checkerboard Metasurface	Comparatively narrow bandwidth	3.8-10.7 GHz (95.17%) (Overall)	Not used for RCS reduction of a patch antenna
[25], 2016	Polarization Converter Metasurface	No significant RCS reduction for a wide band	4.1-12 GHz (98.13%) (Overall)	Co-planar integration of the metasurface
[26], 2016	Polarization Rotator	Narrow Bandwidth for RCS reduction	5.50-8.94 GHz (47.75%) and 13.30-15.50 GHz (16.78 %)	Simple and feasible design, Not used for RCS reduction of a patch antenna
Proposed Design	Polarization Converters	Wideband RCS reduction, In-band as well as Out-of-band RCS reduction, Good RCS reduction at	7.25 GHz -24.83 GHz (110%) (Overall), 10 dB RCS reduction BW 8.33 GHz – 9.16 GHz (9.49 %) and from 12.81 GHz – 18.85 GHz (38.16 %) as compared with the Ref. Patch	Co-planar integration of the metasurface with the patch antenna

	oblique incidence

5.3) Contribution 3: Low-RCS Microstrip Patch Antenna with Artificial Magnetic Conductor Metasurfcae (Design 3)

In this work, Square Patch AMC structures with different dimensions are used to design the Checkerboard metasurface. The main novelty of the proposed design is the use of the same type of Artificial Magnetic Conductor unit cells with different dimensions for achieving wideband Radar Cross Section reduction in contrast to the use of different types of Artificial Magnetic Conductor unit cells.

A square patch structure is used to design the unit cell. The length of the square patch for AMC – I is ls_1 = 1.4 mm and the length of the square patch for AMC – II is ls_2 = 5.3 mm. The dimensions of the unit cells are obtained by extensive parametric analysis to obtain the required phase difference for wideband RCS reduction. The unit cells are designed on FR-4 substrate with thickness h = 2.4 mm, ε_r = 4.3 and loss-tangent tanδ = 0.02. The unit cell has width w = 7 mm. The Copper thickness of 0.035 mm and the unit cell has a metallic ground at the bottom. Fig. 5.3.1 (a) and (b) show the design of the unit cells of AMC I and AMC II respectively.

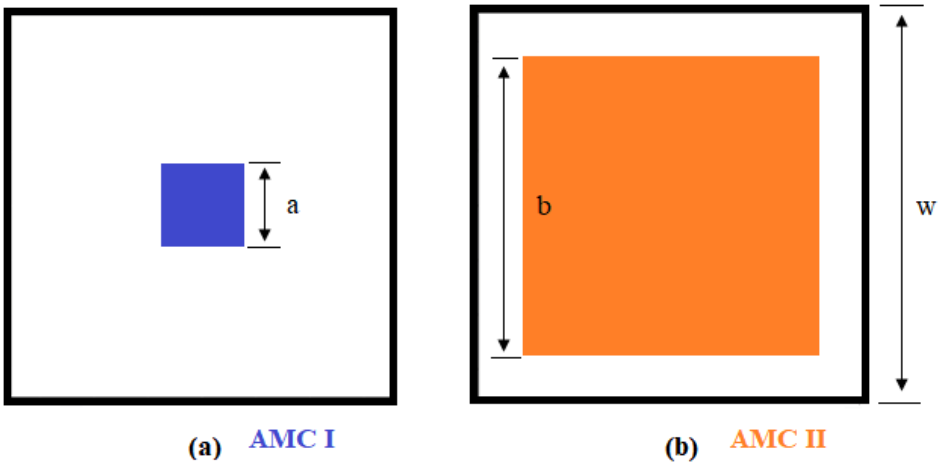

Figure 5.3.1. Design of the AMC unit cell (a) AMC I, (b) AMC II

The simulation of the AMC unit cell is carried out in CST Microwave Studio Software with Periodic Boundary Conditions and Floquet Port excitation with proper de-embedding distance. The unit cell dimensions are optimized in the software to obtain the required phase difference of $180^0 \pm 37^0$ to obtain maximum RCS reduction in the desired frequency range. Fig. 5.3.2 shows the Reflection Coefficient magnitudes of AMC I and AMC II. Fig. 5.3.3 shows the reflection phases of AMC I and AMC II.

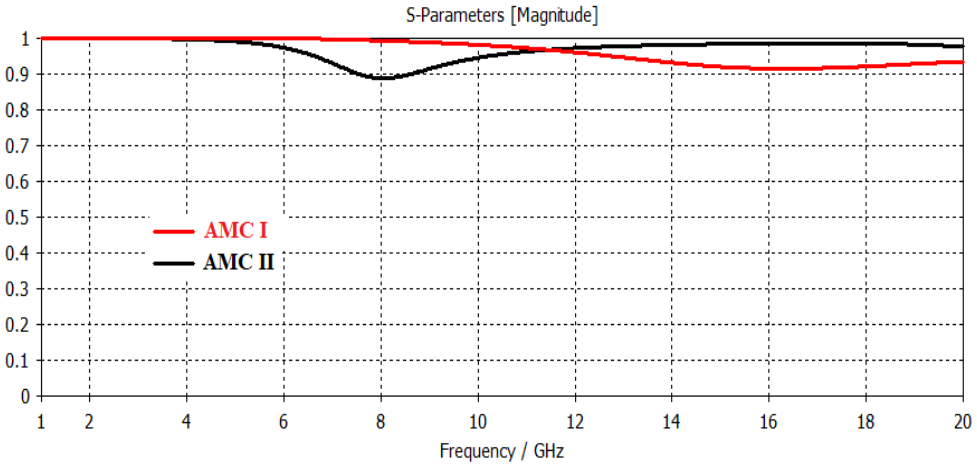

Figure 5.3.2. Reflection Coefficient magnitudes of AMC I and AMC II

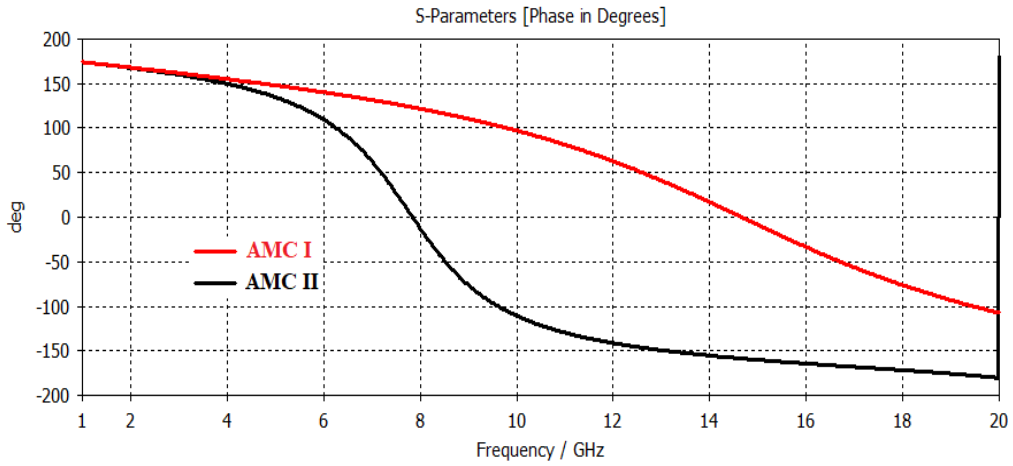

Figure 5.3.3. Reflection Phases of AMC I and AMC II

The resonant frequency of AMC I is 14.726 GHz. Whereas, the resonant frequency of AMC II is 7.857 GHz. From the reflection phase diagrams, it is observed that both the AMCs are single band over the frequency range of 1-20 GHz. The operating bandwidth of AMC I is from 10.46 GHz to 18.83 GHz. The operating bandwidth of AMC II is from 6.48 GHz to 9.32 GHz. Fig. 5.3.4 (a) shows the required phase difference between AMC I and AMC II from which the frequency range for maximum RCS reduction can be predicted. Fig. 5.3.4 (b) shows the predicted 10 dB RCS reduction frequency range of the metasurface. The predicted 10 dB RCS reduction bandwidth is from 8.163 GHz to 15.384 GHz considering infinite arrays.

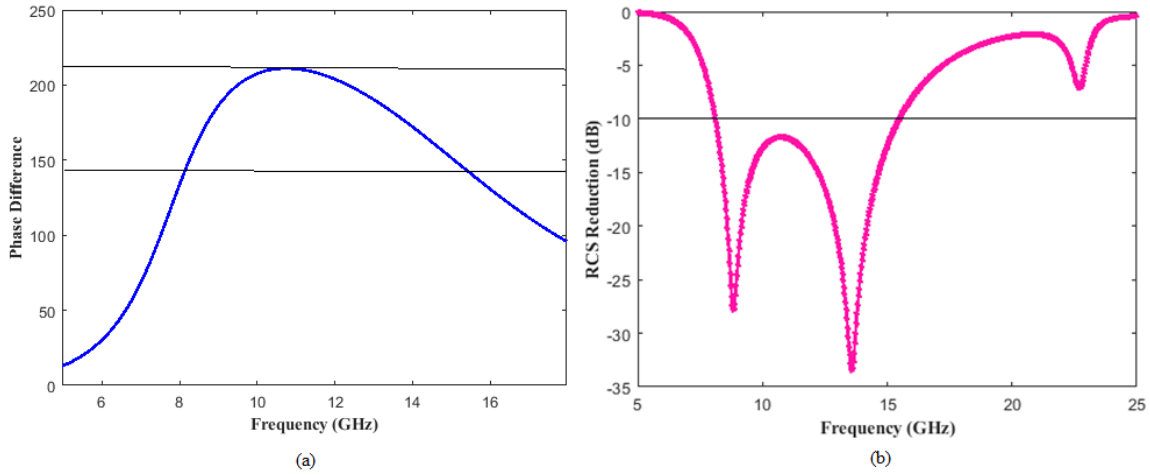

Figure 5.3.4. (a) Phase Difference between AMC I and AMC II, (b) Predicted 10 dB RCS reduction frequency range of metasurface

Fig. 5.3.5 (a) shows the magnitude of Reflection Coefficient of AMC I under oblique incidence for TE mode. It shows that the magnitude of the Reflection Coefficient remains almost the same for the angles on incidence up to 50 Deg. The variation in the magnitude is slight.

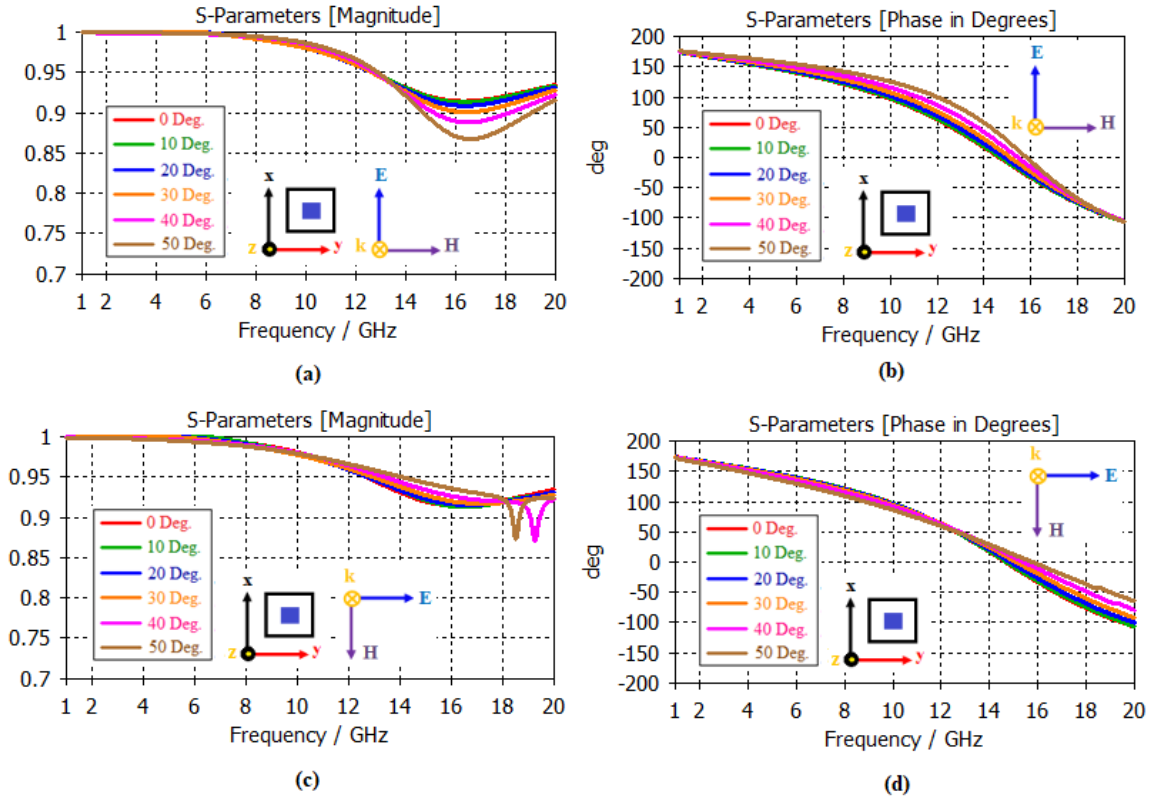

Figure 5.3.5. (a) Reflection Coefficient Magnitudes of AMC I under oblique incidence (TE Mode), (b) Reflection Phase of AMC I under oblique incidence (TE Mode), (c) Reflection Coefficient Magnitudes of AMC I under oblique incidence (TM Mode), (d) Reflection Phase of AMC I under oblique incidence (TM Mode)

Fig. 5.3.5 (b) shows the Reflection Phase of AMC I under oblique incidence for TE mode. The reflection phase response is almost similar for the angles of incidence up to 20 Deg. After that there are negligible variations in the resonant frequency of the AMC. Fig. 5.3.5 (c) shows the Reflection Coefficient magnitude of AMC I for various angles of incidence in the case of Transverse Magnetic (TM) mode. In this mode also, there are negligible variations in the magnitude of the Reflection Coefficient for the frequency range of 1 GHz-20 GHz. The Reflection Phase response of AMC I under oblique incidence for TM mode is shown in Fig. 5.3.5 (d). It shows that the frequency of resonance remains the same for the angles of incidence up to 50 Deg. These responses prove better angular stability of AMC I under oblique incidence for TM mode. So, it can be concluded that the AMC I shows better angular stability for TE as well as TM mode over a wide frequency range.

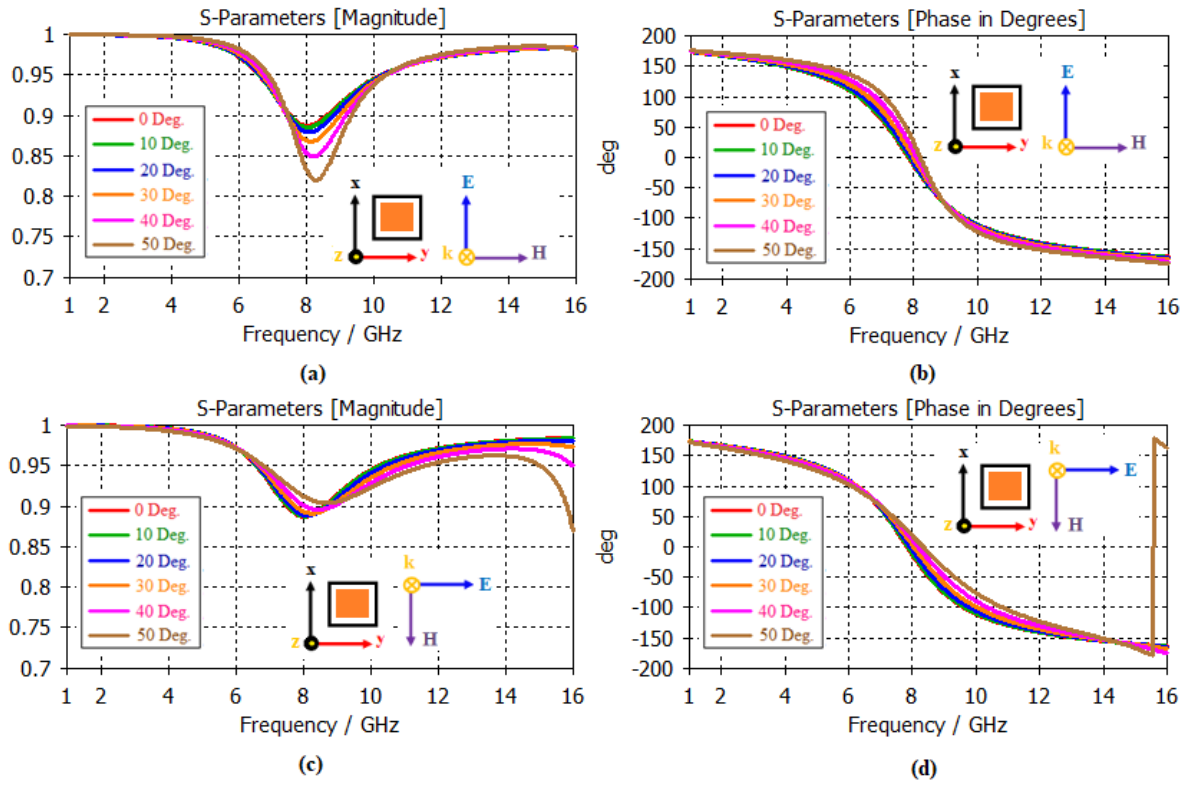

Figure 5.3.6. (a) Reflection Coefficient Magnitudes of AMC II under oblique incidence (TE Mode), (b) Reflection Phase of AMC II under oblique incidence (TE Mode), (c) Reflection Coefficient Magnitudes of AMC II under oblique incidence (TM Mode), (d) Reflection Phase of AMC II under oblique incidence (TM Mode)

Fig. 5.3.6 (a) shows the Reflection Coefficient Magnitudes of AMC II under oblique incidence for Transverse Electric (TE) mode. The simulation results show that AMC II shows good angular stability for angles of incidence up to 40 Deg. if the magnitude of the reflection coefficient is concerned. After 40 Deg., slight changes are observed in the reflection coefficient magnitude. Fig. 5.3.6 (b) shows the reflection phase of the AMC II for oblique

incidence in the case of TE mode. As far as, the reflection phase is concerned, the structure shows good angular stability for angles of incidence up to 40 Deg. However, the zero crossing of the phase curve is observed at the same frequency for the angles of incidence up to 50 Deg. These amplitude and phase responses show better angular stability of AMC II under oblique incidence for TE mode.

Fig. 5.3.6 (c) shows the Reflection Coefficient Magnitudes of AMC II under oblique incidence for TM mode. It shows that the variation in the magnitude of the Reflection Coefficient is negligible for the angles of incidence up to 50 Deg. The Reflection Phase response of AMC II under oblique incidence for TM mode is shown in Fig. 5.3.6 (d). It shows that the frequency of resonance remains almost the same for the angles of incidence up to 40 Deg. At the angle of 50 Deg., the reflection phase response is slightly different after 15 GHz but before that it is almost similar to the other responses. It proves the angularly stable performance of AMC II for TM mode.

Fig. 5.3.7 (a) and Fig. 5.3.7 (b) show two different designs of Checkerboard metasurfaces with 3×3 blocks. In both the designs the positions of blocks of AMC I and AMC II are different. The RCS reduction performance of both the designs is analyzed by numerical simulations in CST Microwave Studio software. Fig. 5.3.7 (c) and Fig. 5.3.7 (d) show the metasurface designs of the Conventional Checkerboard Configuration and the Triangular Checkerboard Configuration respectively.

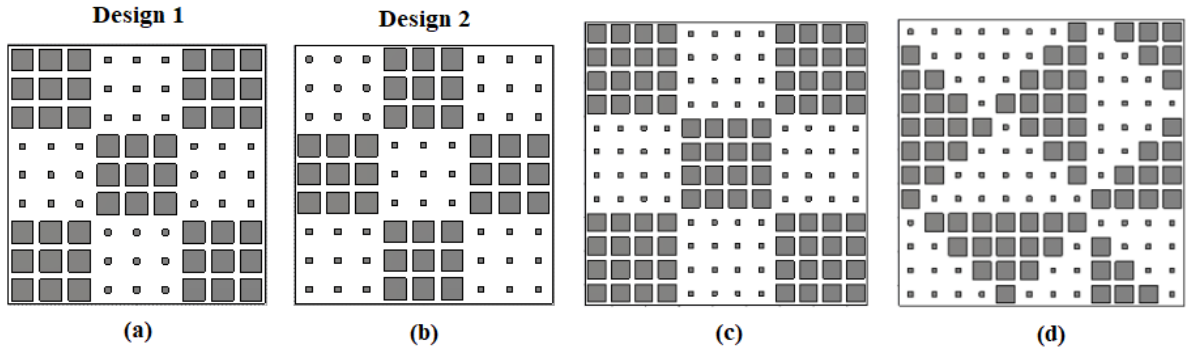

Figure 5.3.7. Designs of Metasurface (a) Design 1, (b) Design 2, (c) CCB Configuration, (d) TCB Configuration

Fig. 5.3.8 (a) shows the simulated RCS values of metasurface Design 1, Design 2 and Metal Sheet. It is inferred from this comparison that Design 2 shows better RCS reduction as compared with Design 1. The RCS values of Design 1 and Design 2 are compared with the metal plate of the same dimensions. Although the Design 2 shows better RCS reduction as compared with Design 1 but overall RCS reduction bandwidth is almost the same for both the designs.

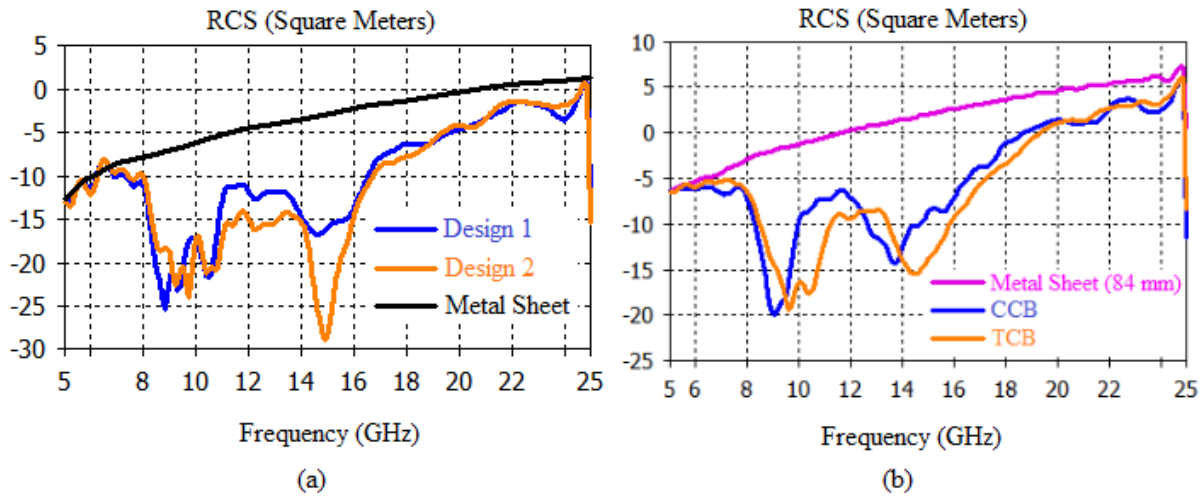

Figure 5.3.8. (a) RCS Comparison of metasurface designs, (b) RCS comparison of the Metal Sheet, CCB Configuration and TCB Configuration

Fig. 5.3.8 (b) shows the RCS characteristics of the Metal Sheet, Conventional Checkerboard Configuration and the Triangular Checkerboard Configuration of a 12 × 12 array of unit cells. The metal sheet has dimensions of 84 mm × 84 mm in this case. It can be inferred that for the metasurfaces with larger dimensions, the TCB Configuration outperforms in terms of 10 dB RCS reduction bandwidth.

The designed metasurfaces can be used to reduce the RCS of a microstrip patch antenna. The coplanar loading technique is used to design the antenna with AMC metasurface. The microstrip antenna is designed on FR-4 substrate with dielectric constant ε_r=4.3, thickness h=2.4 mm and loss tangent tanδ=0.02. The Cu thickness is 0.035 mm. The dimensions of the square patch antenna are 7 mm × 7 mm. The ground plane and the substrate length and width are lg = 63 mm and wg = 63 mm respectively. Initially the metasurface was designed and its RCS reduction performance is evaluated. Then the 3 × 3 array of unit cells is removed from the center to facilitate the patch antenna design. The patch antennas are excited with coaxial feed. Two types of antenna designs were investigated based on the arrangement of AMC unit cells.

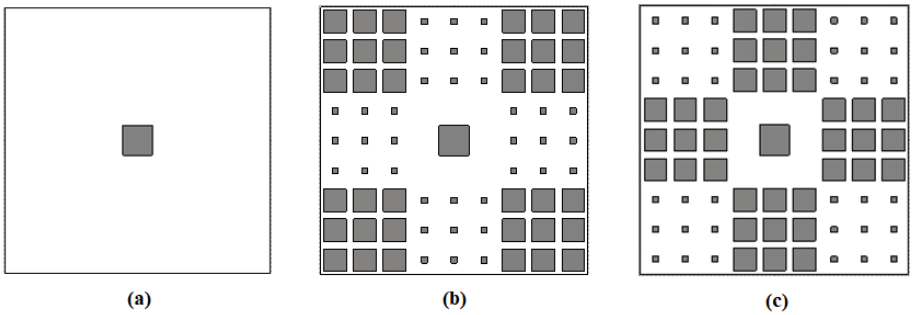

Figure 5.3.9. (a) Ref. Patch Antenna; Microstrip antenna with AMC Metasurface (b) Design 1, (c) Design 2

Fig. 5.3.9 (a) shows the Reference Patch Antenna design. Fig. 5.3.9 (b) and Fig. 5.3.9 (c) show the antenna designs with AMC Checkerboard Metasurfaces. In Design 1, the AMC II is placed at the four corners of the substrate whereas in Design 2 the positions of AMC I and AMC II are interchanged. The RCS reduction performance of both the designs is investigated through numerical simulations. It was observed that the RCS reduction performance of Design 1 is better than that of the Design 2. In the case of metasurface Design 2 showed better RCS reduction but due to the removal of 3 × 3 array from the center, the destructive interference is modified and Design 1 shows better performance as compared to Design 2. Design 1 is written as Antenna 1 and Design 2 is written as Antenna 2. The Triangular Checkerboard Configuration (TCB) was also examined which showed the 10 dB RCS reduction performance similar to that of the predicted 10 dB RCS reduction frequency range. The top views of the fabricated Reference Patch Antenna and the Antenna 1 with AMC are shown in Fig. 5.3.10 (a) and Fig. 5.3.10 (b) respectively.

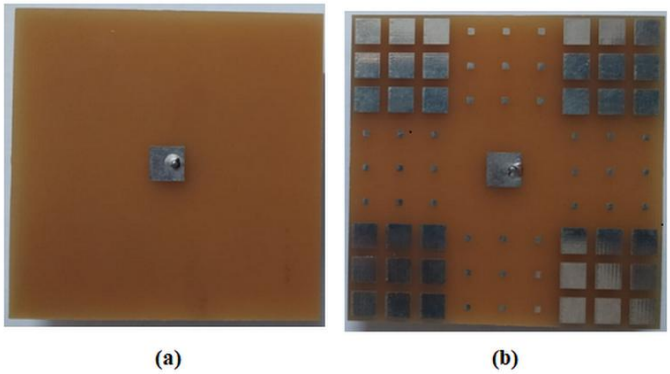

Figure 5.3.10. Fabricated Patch Antennas (a) Reference Patch, (b) Antenna with AMC

The simulations of the RCS reduction performance and the parameters like Gain, Reflection Coefficients and radiation patterns are carried out in CST Microwave Studio software. The simulated results are also verified with experimental measurements. Fig. 5.3.11 shows the RCS responses of the Antenna 1, Antenna 2, Reference Patch and Metal Sheet. The proposed design of Antenna 1 shows overall RCS reduction bandwidth of 6.93 GHz – 24.59 GHz (112.06 %) as compared with the metal sheet and the Reference Patch. 10 dB RCS reduction is obtained from 8.317 GHz – 11.317 GHz (30.56 %) and from 13.22 GHz – 16.146 GHz (19.93 %) as compared with the metal sheet. If the results are compared with the Reference Patch Antenna, then 10 dB RCS reduction is obtained from 8.317 GHz – 11.317 GHz (30.56 %) and from 13.183 GHz – 16.183 GHz (20.43 %) as compared with the Reference Patch Antenna. The RCS response of the design is same for TE mode as well as TM mode due to structural symmetry. For the Design 1, the RCS reduction peaks are

observed at 8.68 GHz (-29.03 dBsm), 9.71 GHz (-39.34 dBsm), 10.71 GHz (-25.765 dBsm) and 14.33 GHz (-36.53 dBsm).

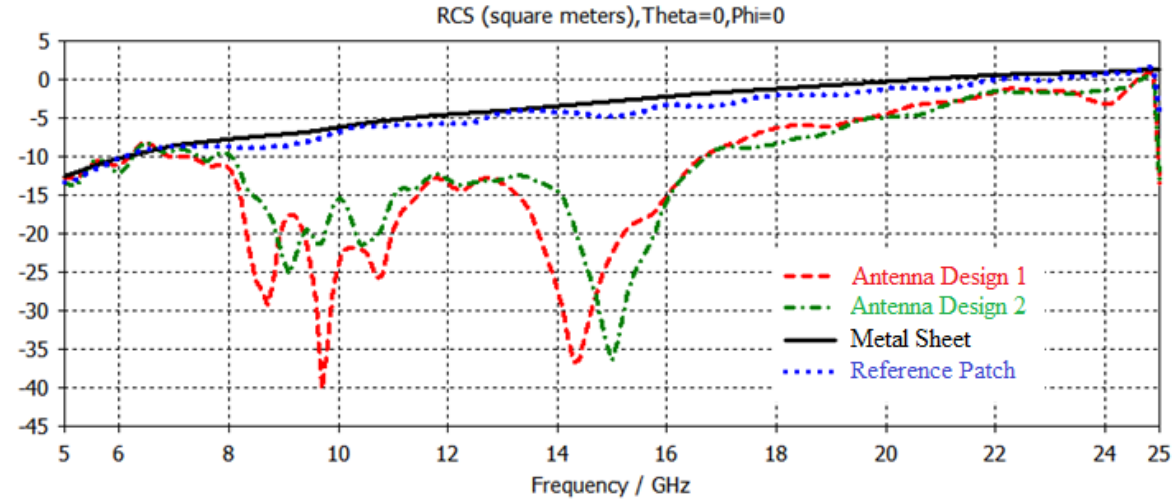

Figure 5.3.11. RCS comparison of Design 1, Design 2, Metal Sheet and Reference Patch (TE, TM Modes)

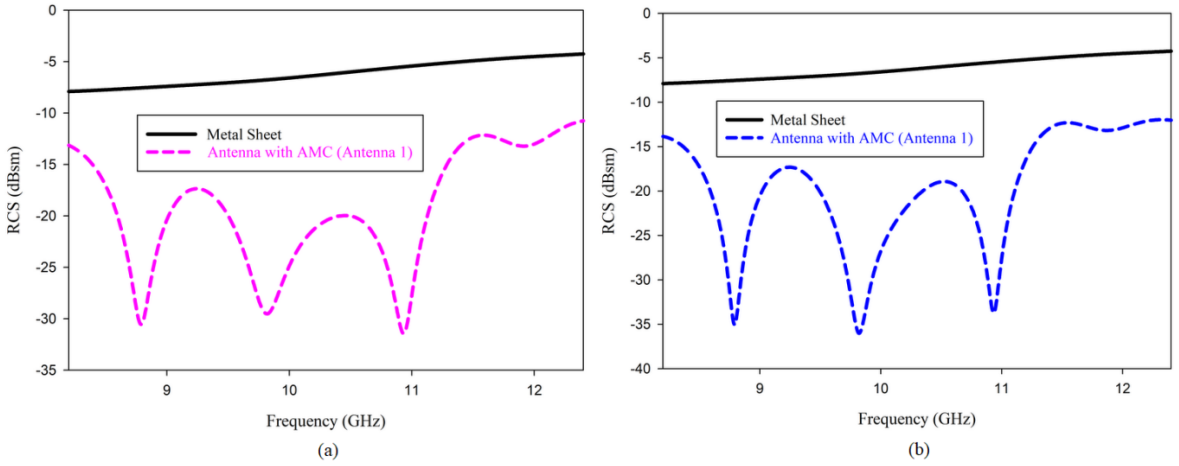

Figure 5.3.12. Experimentally measured RCS of Metal Sheet and Antenna with AMC (Antenna 1) (a) TE Mode, (b) TM Mode

Fig. 5.3.12 (a) and Fig. 5.3.12 (b) show the experimentally measured RCS of Metal Sheet and the proposed Antenna with AMC for TE Mode and TM Mode respectively. The results are measured experimentally for the frequency range of 8.2 – 12.4 GHz. The results show that the RCS reduction peaks are obtained at 8.79 GHz (-30.55 dBsm), 9.82 GHz (-29.53 dBsm) and 10.94 GHz (-31.43 dBsm). The same are obtained at 8.8 GHz (-34.86 dBsm), 9.82 GHz (-36.01 dBsm) and 10.94 GHz (-33.74 dBsm) for TM mode. The experimental results are in well agreement with the simulated results.

Fig. 5.3.13 (a) shows the simulated Reflection Coefficients of the Ref. Patch Antenna and Antenna 1. Fig. 5.3.13 (b) and Fig. 5.3.13 (c) show the experimentally measured Reflection Coefficients of the Ref. Patch Antenna and Antenna 1 respectively. The simulated

Reflection Coefficient of the Reference Patch Antenna is around -41.76 dB at the frequency of resonance. The experimentally measured reflection coefficient of the Reference Antenna is around -28 dB at the resonant frequency of the antenna. The simulated Reflection Coefficient of Antenna with AMC has the magnitude of -29 dB at the resonant frequency. The experimentally measured Reflection Coefficient of the same antenna has the value of -29.4 dB at the resonant frequency of 8.6 GHz.

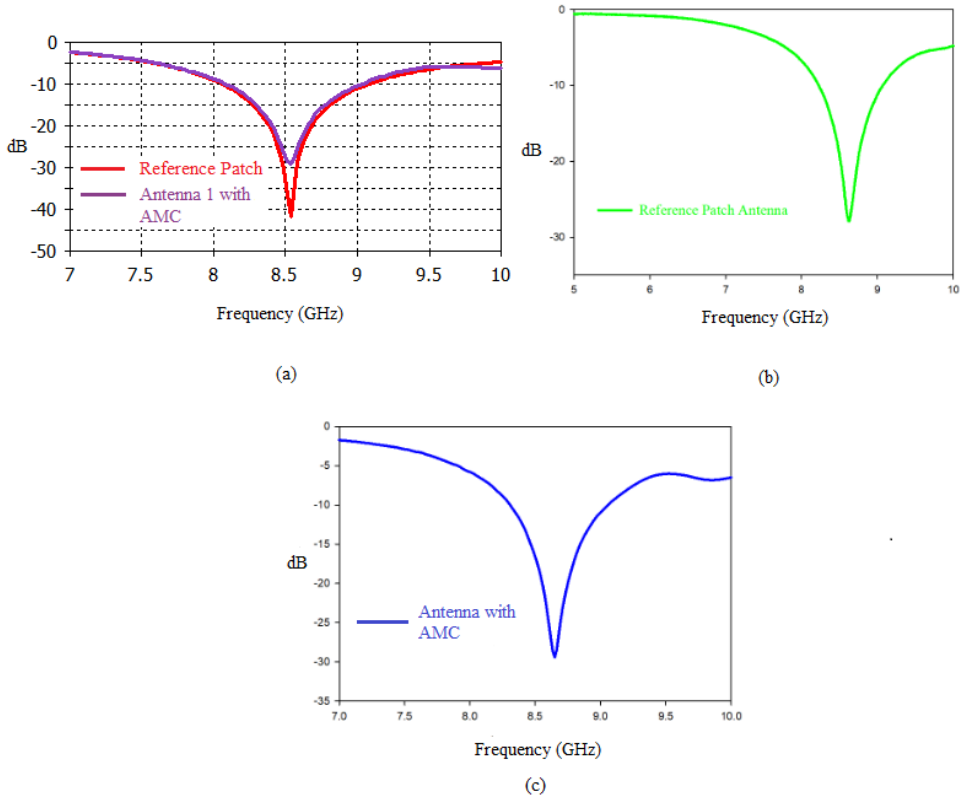

Figure 5.3.13. (a) Simulated Reflection Coefficients of Ref. Patch Antenna and Antenna with AMC (Antenna 1), (b) Experimentally measured Reflection Coefficient of Ref. Patch Antenna, (c) Experimentally measured Reflection Coefficient of Antenna with AMC (Antenna 1)

Fig. 5.3.14 (a) and Fig. 5.3.14 (b) show the gain pattern of the Ref. Antenna in ϕ = 0 Deg. plane (E-plane) and ϕ = 90 Deg. plane (H-plane). Fig. 5.3.14 (c) and Fig. 5.3.14 (d) show the gain pattern of the Antenna with AMC (Antenna 1) in ϕ = 0 Deg. plane (E-plane) and ϕ = 90 Deg. plane (H-plane). The simulated results show that the Ref. Antenna shows the peak gain of 5.52 dB in the ϕ = 0 Deg. plane and 2.5 dB in the ϕ = 90 Deg. plane. The peak gain of the Antenna 1 is 7.24 dB in the ϕ = 0 Deg. Plane and 7.15 dB in the ϕ = 90 Deg. plane. The main lobe of the Antenna 1 is directed almost at 0 Deg. in both the planes. Fig. 5.3.14 (e) and Fig. 5.3.14 (f) show the experimentally measured radiation patterns of the Reference Antenna in ϕ=0 Deg. plane and ϕ=90 Deg. plane respectively. Fig. 5.3.14 (g) and Fig. 5.3.14 (h) show the experimentally measured radiation patterns of the Antenna with AMC (Antenna 1) in ϕ=0 Deg. plane and ϕ=90 Deg. plane respectively. The measurement

is done from -90 Deg. to +90 Deg. due to the limitations in the rotation angles of the positioner. The experimentally measured results show that the radiation patterns of the Antenna with AMC (Antenna 1) do not degrade.

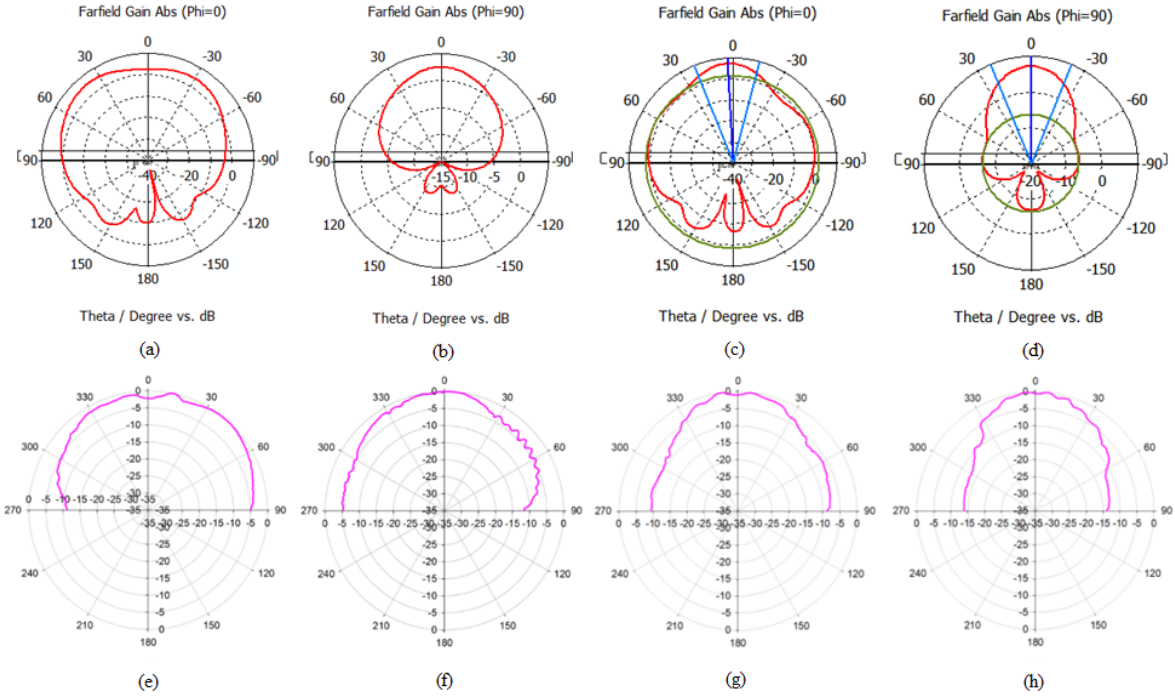

Figure 5.3.14. Gain Patterns of Ref. Antenna in (a) ϕ = 0 Deg. Plane, (b) ϕ = 90 Deg. Plane; Gain Patterns of Antenna with AMC, (c) ϕ = 0 Deg. Plane, (d) ϕ = 90 Deg. Plane; Experimentally measured Radiation Patterns of Ref. Antenna for (e) $\phi = 0^o$ Cut, (f) $\phi = 90^o$ Cut; Experimentally measured Radiation Patterns of Antenna with AMC (Antenna 1) for (g) $\phi = 0^o$ Cut, (h) $\phi = 90^o$ Cut

In the case of Antenna 2, the same resonant frequency is observed but the radiation pattern of Antenna 2 degrades as compared with Antenna 1. The radiation pattern of Antenna 2 is affected due to coupling of metasurface elements with the patch antenna at the resonant frequency. So, to obtain proper radiation patterns Antenna 1 is selected as the proposed design. The simulated surface current distribution shows that there is less coupling of the patch antenna with AMC unit cells in the case of Antenna 1. Whereas Antenna 2 shows strong coupling of the patch antenna with AMC unit cells. Because of this the radiation pattern of Antenna 2 degrades. So, Antenna 1 is selected as the proposed design.

Figure 5.3.15 (a) and (b) show the normalized Co-polar and Cross-polar radiation patterns of the Reference Patch in Ludwig III Co-ordinate system respectively. Similarly, Figure 5.3.15 (c) and (d) show the normalized Co-polar and Cross-polar radiation patterns of Antenna with AMC (Antenna 1) respectively. The radiation diagrams verify the performance of the designed antennas. The Cross-polar patterns can also be plotted in Ludwig II Az/El or Ludwig II El/Az Co-ordinate systems.

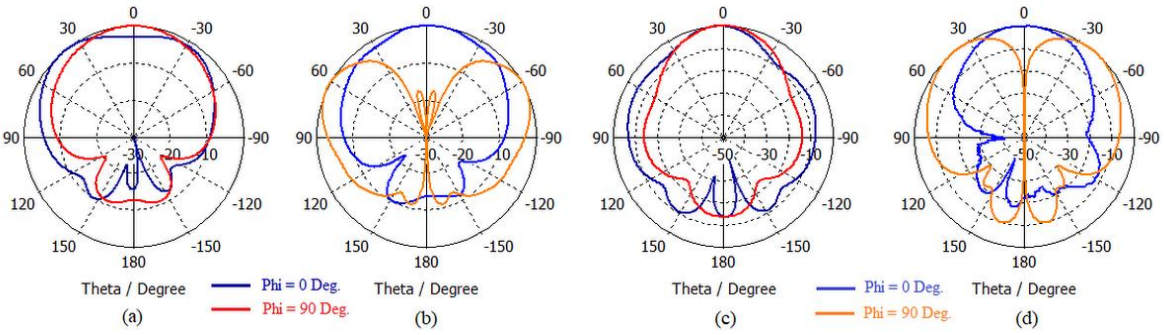

Figure 5.3.15. Normalized Copolar and Crosspolar Radiation Patterns in Ludwig III Co-ordinate system (a) Ref. Patch Co-polar, (b) Ref. Patch Cross-polar, (c) Antenna with AMC Co-polar, (d) Antenna with AMC Cross-polar

Fig. 5.3.16 (a) shows the Bistatic Scattering RCS comparison of the Metal Sheet, Reference Patch and Antenna 1 with AMC in the ϕ=0 Deg. plane at the frequency of 9.7 GHz. The figure shows the strong main lobe in the boresight direction in the cases of Metal Sheet and Ref. Patch. The RCS values of the Metal Sheet, Ref. Patch and Antenna 1 at θ=0 Deg. are -6.48 dBsm, -7.53 dBsm and -40.1 dBsm respectively in the ϕ=0 Deg. Plane.

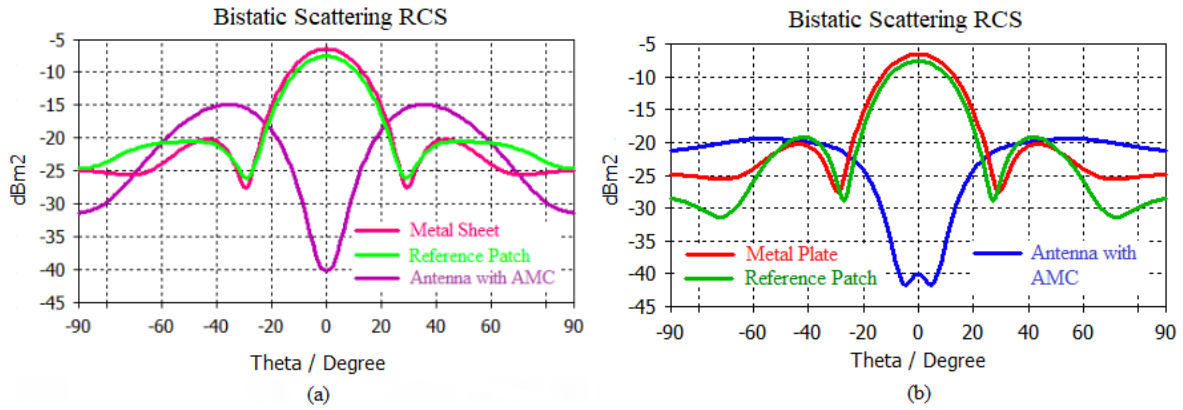

Figure 5.3.16. Bistatic Scattering RCS comparison at 9.7 GHz (a) ϕ=0 Deg. (b) ϕ=90 Deg.

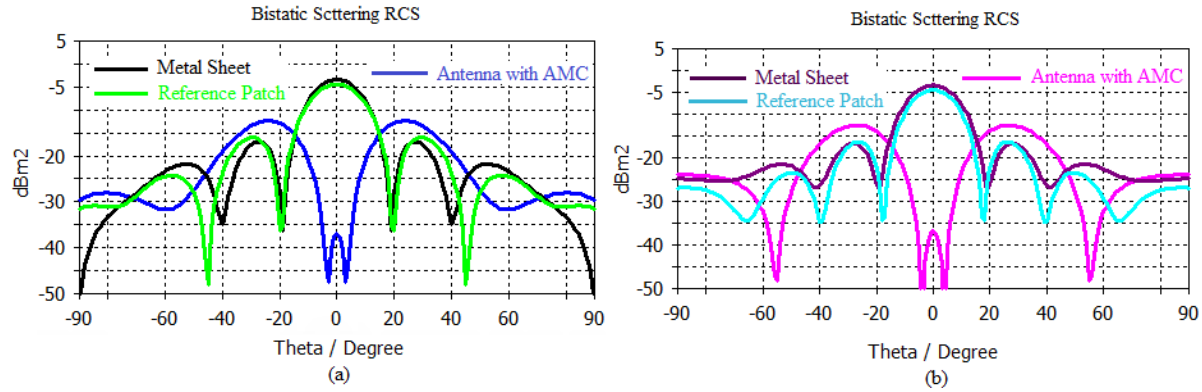

Figure 5.3.17. Bistatic Scattering RCS comparison at 14.38 GHz (a) ϕ=0 Deg., (b) ϕ=90 Deg.

The Antenna 1 shows RCS reduction of 33.62 dBsm and 32.57 dBsm in the normal direction as compared with the Metal Sheet and the Ref. Patch respectively. Within the

angular range of ± 20 Deg., considerable main lobe suppression is observed for the Antenna 1. Fig. 5.3.16 (b) shows the Bistatic Scattering RCS comparison of the samples in the ϕ=90 Deg. plane at the same frequency. Figure 5.3.17 (a) shows the Bistatic Scattering RCS comparison of the samples at 14.38 GHz in the ϕ=0 Deg. Plane. The RCS values of the Metal Plate, the Reference Antenna and Antenna 1 with AMC are -3.3 dBsm, -4.4 dBsm and -36.86 dBsm respectively in the ϕ=0 Deg. plane. The Antenna with AMC shows RCS reduction of 33.56 dBsm and 32.46 dBsm with respect to the Metal Sheet and the Reference Patch. Figure 5.3.17 (b) shows the Bistatic RCS comparison at 14.38 GHz in the ϕ =90 Deg. Plane. The RCS reduction of the Antenna 1 with AMC is verified in this plane also.

Fig. 5.3.18 (a), (b) and (c) show the 3D scattered field from the Metal Sheet, Ref. Patch and Antenna 1 with AMC. The scattered fields show that the Metal sheet and the Ref. Patch have stronger major lobes in the boresight direction. But, in the case of Antenna 1 with AMC, the major lobe is suppressed in the normal direction and the fields are scattered in the various directions. It makes Antenna 1 imperceptible and reduces its radar signature.

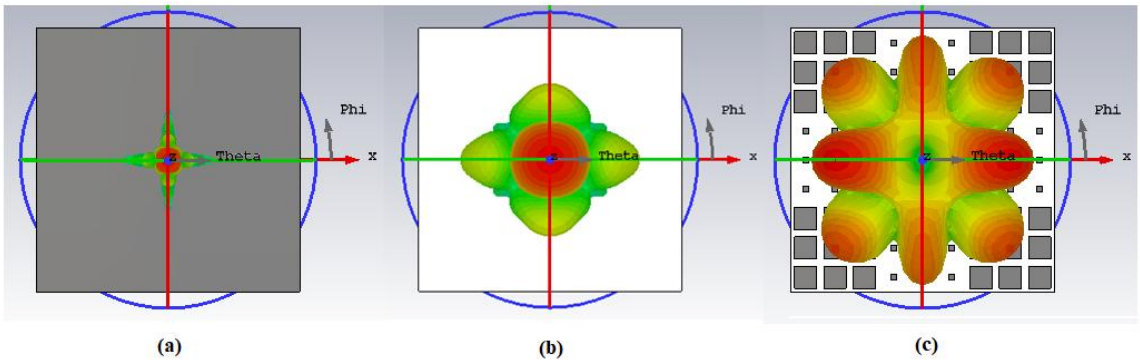

Figure 5.3.18. 3D Bistatic Scattering at 9.7 GHz; (a) Metal Sheet, (b) Ref. Patch, (c) Antenna 1 with AMC

The comparison of the proposed design with existing state-of-the art is presented in Table 5.3.1. The comparison is done in terms of Percentage Bandwidth of RCS reduction, angular stability, design complexity and methodologies for achieving RCS reduction. The comparison shows that the proposed design offer wide RCS reduction bandwidth, angular stability for TE and TM modes, enhancement in Radiation Pattern and less fabrication complexity. Bistatic RCS reduction can also be achieved with the proposed design.

Table 5.3.1. Comparison of the proposed design with similar work

Ref. , Year of Publication	**Methodology Used**	**Limitations**	**Per. Bandwidth**	**Design Complexity**
[27], 2020	Triangular Checkerboard	Less angular stability after 40	59 GHz – 73 GHz (21.2%) (-8 dB)	Single Layer Design

	Surface	deg. angle of incidence, Not used for RCS red. of an antenna		
[28], 2018	Polarization rotator with MEMS switch	Not used for RCS reduction, Angular stability isn't mentioned	7.93 GHz-12.42 GHz (44.13%) for LP to LP, 8.07 GHz - 10.77 GHz (28.66%) for LP to CP	Complex Design due to the inclusion of MEMS switch
[29], 2017	Diffuse Metasurface	Narrow BW, Not integrated with an antenna	5.4 GHz- 7.4 GHz (31.25%)	Ergodic optimization based design
[30], 2015	Chessboard superstrate with Fabri-Parot Cavity	Increases the height of the antenna	8-14 GHz (54.5%) (Overall)	Two-layer structure
[31], 2021	Polarization Converter Metasurface	Not used for RCS reduction of Antenna	8.6 GHz – 22 GHz (88%)	Planar Configuration
[32], 2018	Polarization Rotation Reflective Metasurface (PRRM)	Tilted rad. pattern for LHCP mode, Angular stability of the unit cell was not discussed	6.5-22 GHz (108.77%) (Overall) 7.55 GHz – 20.74 GHz (93.25%) (11 dB Average RCS reduction)	Coplanar integration of the metasurface
Proposed Design III using AMCs (FR-4)	Artificial Magnetic Conductors (AMC)	Wideband RCS Reduction for TE as well as TM polarizations, In-band as well as out-of-band RCS reduction	Overall RCS reduction BW [6.93 GHz – 24.59 (112.06 %)], 10 dB RCS reduction BW [8.317 GHz – 11.317 GHz (30.56 %) and from 13.22 GHz – 16.146 GHz (19.93 %)] as compared with PEC	Checkerboard Configuration

The comparison shows that the proposed design offer wide RCS reduction bandwidth, angular stability for TE and TM modes, enhancement in Radiation Pattern and less fabrication complexity.

5.4) Contribution 4: Microstrip Patch Antenna with Jerusalem Cross Slots in the Ground Plane

The Jerusalem cross type structure is well known frequency selective surface. It is a type of Artificial Magnetic Conductor which offers high impedance. High impedance surfaces (HIS) are used to suppress the surface waves. Because of these characteristics, resonator length can be reduced and antenna miniaturization becomes possible.

By etching Jerusalem Cross structure in the ground plane, Size and Radar Cross Section of an antenna can be reduced significantly. In addition to this, considerable reduction in antenna size can be observed without degradation of antenna parameters. The conventional half-wavelength size of the resonator is reduced by a factor $\sqrt{(\varepsilon_{eff} * \mu_{eff})}$. Where ε_{eff} and μ_{eff} indicate effective permittivity and effective permeability respectively. The dimensions of the structure and the resonant frequency can be calculated by parametric analysis or suitable optimization process.

The patch antenna is designed to resonate at 2.4 GHz. The antenna is fabricated with FR-4 substrate with $\varepsilon_r = 4.4$. The height of the substrate h is taken as 0.8 mm. The length and the width of the conventional square patch antenna are 30.14 mm (0.24λ). The parameter λ is the resonant wavelength of the antenna. The ground size is 34.94 mm × 34.94 mm. The feed is 8.688 mm long and 0.648 mm wide. The inset depth is found to be 6.288 mm. The dimensions of the inset gap are optimized to obtain the minimum Reflection Coefficient. Fig. 5.4.1 (a) shows the structure of the Jerusalem Cross Unit Cell.

Fig. 5.4.1 (b) shows the ground plane of the modified antenna with Jerusalem Cross Slots. The dimensions of the unit cell of the Jerusalem Cross structure are as follows; unit cell size = 7 mm, W = 5.5 mm, inter element spacing of the JC structure g = 0.5 mm, End Capacitor width = 0.4 mm, length l = 5.7 mm and width w = 0.25 mm. The length of the ground plane of the modified antenna is optimized at 40 mm and the width is kept at 22 mm for maintaining the antenna performance. A 3 × 3 array of Jerusalem Cross type of slots is etched in the ground plane of the modified antenna as shown in Fig. 5.4.1 (b) and the patch antenna dimensions are optimized to get the same resonant frequency.

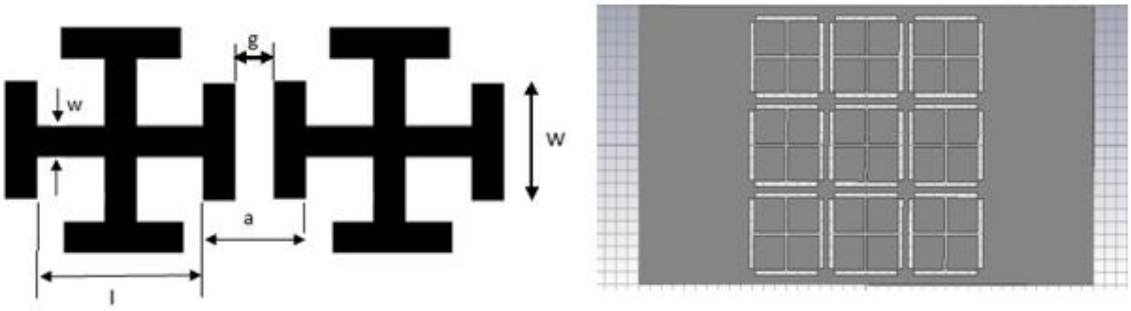

Figure 5.4.1 (a) Jerusalem Cross Structure, (b) Microstrip patch antenna loaded with Jerusalem Cross Structure (Bottom View)

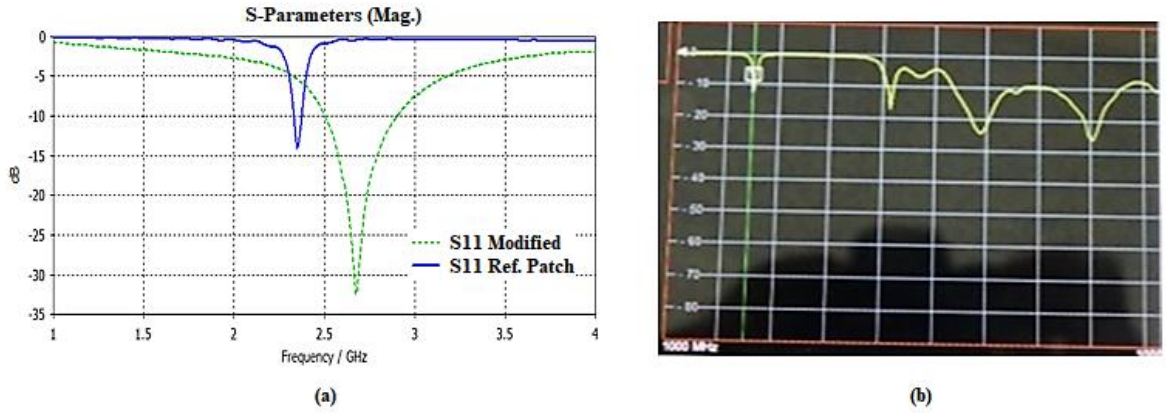

Figure 5.4.2 (a) Simulated Reflection coefficient of the conventional and the modified patch antenna (b) Measured Reflection coefficient of the conventional antenna

The miniaturized patch antenna has dimensions of 16.7 mm × 16.7 mm i.e. 0.145λ × 0.145λ. It is observed from the Figure 5.4.2 (a) that the conventional patch antenna resonates at around 2.4 GHz. The minimum value of Reflection coefficient is nearly -14 dB. The resonant frequency of the Metasurface loaded antenna is around 2.6 GHz which is almost the same as that of the conventional antenna. From simulation results it can be observed that the Reflection coefficient of the modified antenna is around -33 dB at the resonant frequency**.** So a significant improvement in the Reflection coefficient performance can be observed. The -10 dB impedance bandwidth is also increased for the JC loaded antenna since the Quality Factor of the antenna reduces owing to the change in effective permeability and permittivity values. The fabricated antennas were tested on Anritsu S820E Vector Network Analyzer for Reflection Coefficient. The measured Reflection Coefficient of the conventional antenna was nearly -12 dB as shown in Figure 5.4.2 (b).

Figure 5.4.3 shows the monostatic Radar Cross Section of the conventional patch antenna for the plane wave incident at θ=0 deg. From 3 GHz to 10 GHz the value of RCS remains in the vicinity of -20 dB. The minimum value over this band is around -22 dB. It also compares the RCS of the conventional antenna with the modified antenna. The RCS of the modified antenna is reduced considerably as shown in this figure. The RCS reduction peaks are observed at 3.12 GHz, 4.52 GHz and 5.51 GHz. The values of RCS are -28.03 dBsm, -27.46 dBsm and -24.25 dBsm at these frequencies respectively. Overall RCS reduction bandwidth is 3 GHz – 10 GHz.

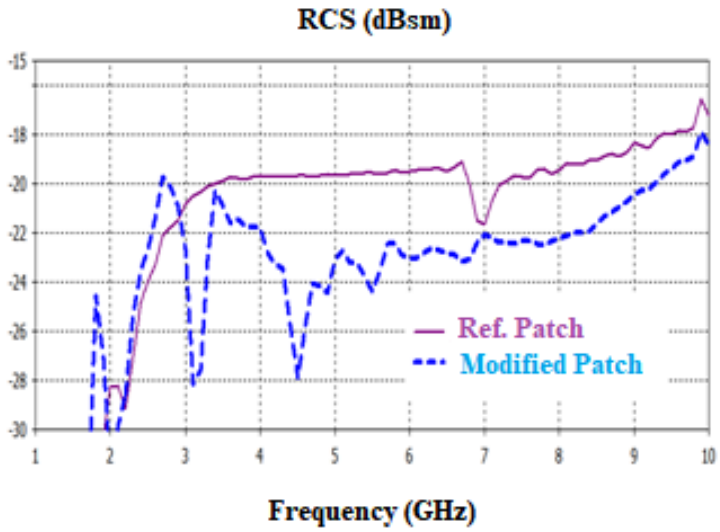

Figure 5.4.3. Radar Cross Section of conventional and modified patch antenna at θ=0 deg.

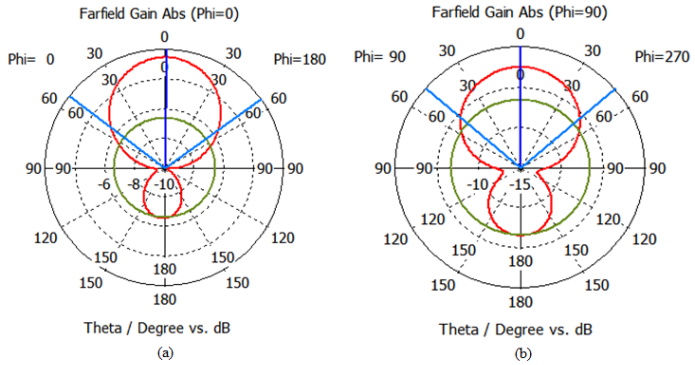

Figure 5.4.4. Gain patterns for the conventional antenna at a) ϕ=0˚, b) ϕ=90˚

Figure 5.4.4 shows the gain values in both the principal planes for the conventional patch antenna resonating at 2.4 GHz. Since FR-4 is a lossy substrate, the gain of the Reference Antenna is low. Because of its lower directivity, the Half Power Beamwidth in both the principal planes is 107.1 deg. and 98.1 deg. respectively.

The orientation of electric field of the incident wave may change. The incident angle of the plane wave is made 60 deg. and RCS of the conventional antenna is compared with the RCS of the modified antenna for the same angle of incidence as shown in Figure 5.4.5 (a). It is observed that monostatic RCS of the conventional antenna remains between -30 dBsm to -37 dBsm from 3-10 GHz**.** The modified antenna is also excited with a plane wave incident at 60 deg. The minimum value of RCS obtained is around -47.28 dBsm at 4.52 GHz**.** The RCS reduction peaks are observed at 2.82 GHz (-42.82 dBsm), 4.32 GHz (-45.24 dBsm), 4.52 GHz (-47.28 dBsm) and at 5.5 GHz (-40.12 dBsm). From the RCS graph, it is evident that a considerable reduction of Radar Cross Section can be obtained for the frequency range of 3-10 GHz which was not the case for the conventional antenna.

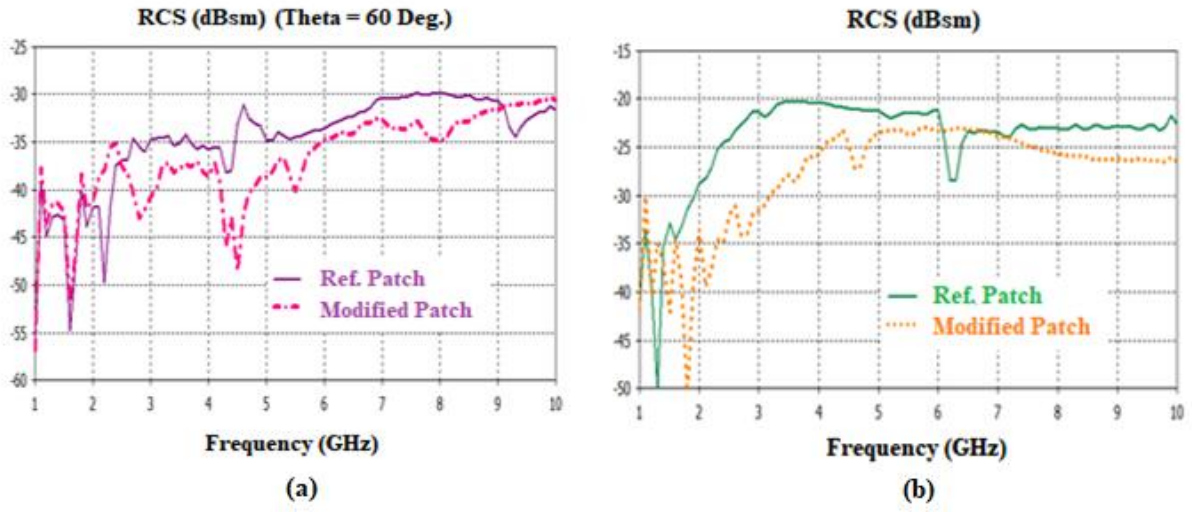

Figure 5.4.5. (a) Monostatic RCS of the structure when the plane wave is incident at 60 deg., (b) RCS for wave incident at θ=15 deg. and E-plane rotated at 90 deg. for the conventional and modified antenna

In Figure 5.4.5 (b), the E-plane of the incident wave is rotated by 90 deg. and RCS characteristics are obtained. The angle of incidence of the plane wave is 15 deg. The RCS values remain within -20 dB to -28 dB from 3 GHz to 10 GHz frequency range for the conventional antenna. For the modified antenna RCS is significantly reduced for the same incident angle. If the frequency band of 1-3 GHz is considered, then RCS is reduced significantly and the minimum value is found to be -50.16 dBsm. The RCS reduction peaks are observed at 1.8 GHz (-50.16 dBsm), 2.13 GHz (-39 dBsm) and at 2.76 GHz (-33.98 dBsm).

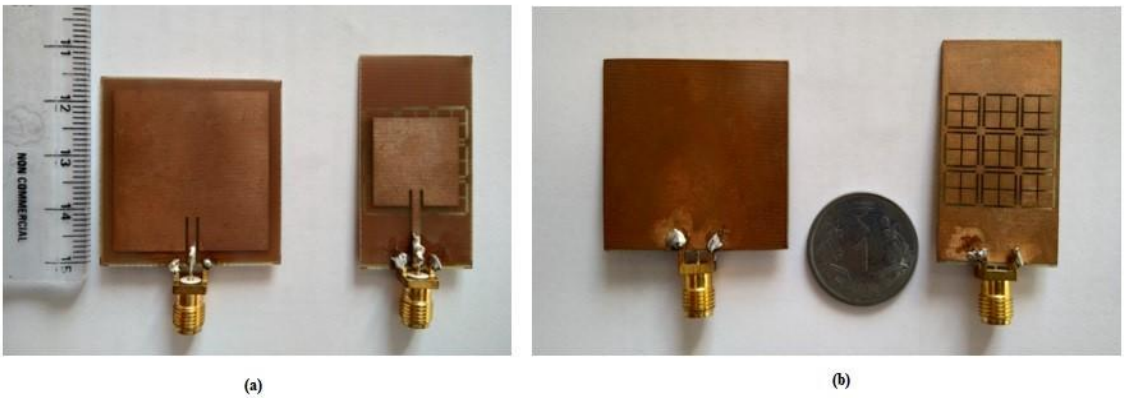

Figure 5.4.6. (a) Fabricated patch antennas (Top View), (b) Fabricated patch antennas (Bottom View)

Figure 5.4.6 (a) and Figure 5.4.6 (b) show the photographs of the fabricated conventional and modified microstrip antennas. Inset feed is used to excite the microstrip patch antenna. The measured Reflection coefficient for the antenna loaded with JC structure was nearly -29 dB, which is in well agreement with the simulated results.

From the simulation results of effective permittivity and effective permeability it is verified that the values of ε_{eff} and μ_{eff} are changed at the resonant frequency**.** So miniaturization factor $\sqrt{(\varepsilon_{eff*}\mu_{eff})}$ increases and the size of the patch antenna is reduced. The patch size can be reduced by 44.59%. The main reason for antenna miniaturization is the shift in the resonant frequency. If the 3 × 3 array of Jerusalem Cross Slots is created in the ground plane of the conventional patch antenna, then the resonant frequency of the patch antenna reduces and it shifts to the left side. To obtain the original resonant frequency of 2.4 GHz, the dimensions of the patch antenna should be reduced. Because of this size reduction the Radar Cross Section of the modified antenna decreases considerably. The negative values of permittivity and permeability confirmed the metasubstrate behavior.

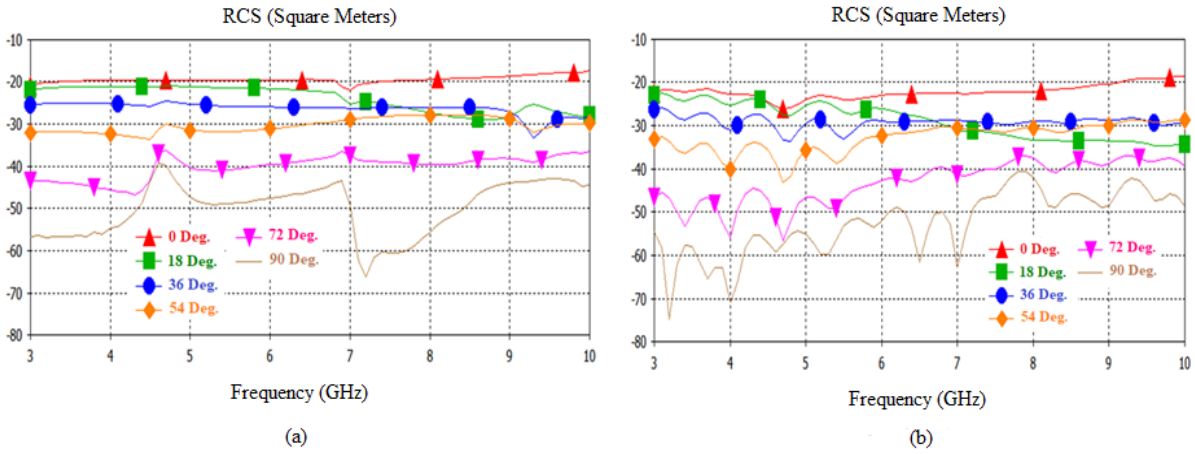

Figure 5.4.7. (a) Radar Cross Section of the conventional patch antenna at different angles of plane wave, (b) Radar Cross Section of Jerusalem Crosses loaded patch antenna at different angles of plane wave

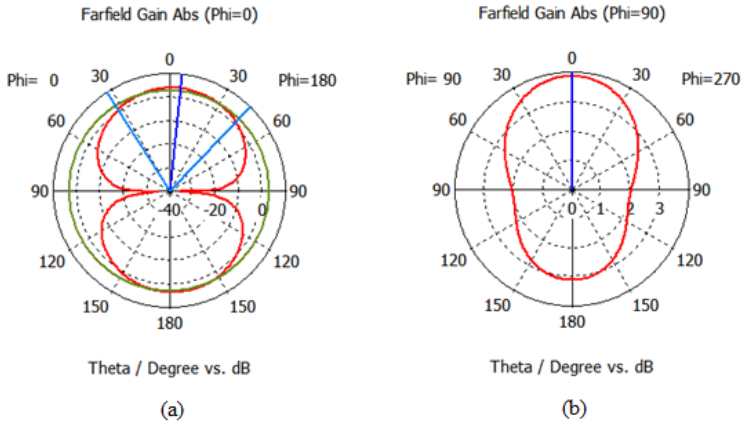

Figure 5.4.8. Gain patterns for the modified antenna at a) ϕ = 0˚, b) ϕ = 90˚

Finally, parametric study for the plane wave angle of incidence is carried out for the conventional antenna as shown in Figure 5.4.7 (a). The parametric study is carried out in CST Microwave Studio software. Referring to Figure 5.4.7 (b), it can be concluded that if the

angle of incidence is changed then RCS reduction can be observed in the case of modified antenna.

After suitable optimization of the geometry, the gain value of 3.94 dB is obtained in one principal plane while 3.87 dB is observed in the orthogonal plane, which shows gain enhancement as compared with the conventional structure. Observing the radiation diagrams, it is evident that there is a significant improvement of gain for the resonant frequency of 2.68 GHz. Figure 5.4.8 (a) and Figure 5.4.8 (b) show the gain patterns of the modified antenna in both the principal planes.

Figure 5.4.9 (a) and Figure 5.4.9 (b) show the measured radiation patterns of the conventional antenna. Figure 5.4.10 (a) and Figure 5.4.10 (b) show the measured radiation patterns for the antenna loaded with JC-slots. The co-polar and cross-polar radiation patterns were obtained at 10 frequency points for the scan angles of -90 deg. to +90 deg. Measured results show that the modified antenna does not show pattern degradation. Gain transfer technique was used to measure the gain of both the antennas. Peak gain has been measured for both the antennas. At the resonance frequency, the measured gain value for the conventional antenna was -2.68 dB in the boresight direction. The gain value for the modified antenna was 1.05 dB in the same direction considering uncertainty level of ±1 dB. Hence the gain was improved as compared with the conventional antenna.

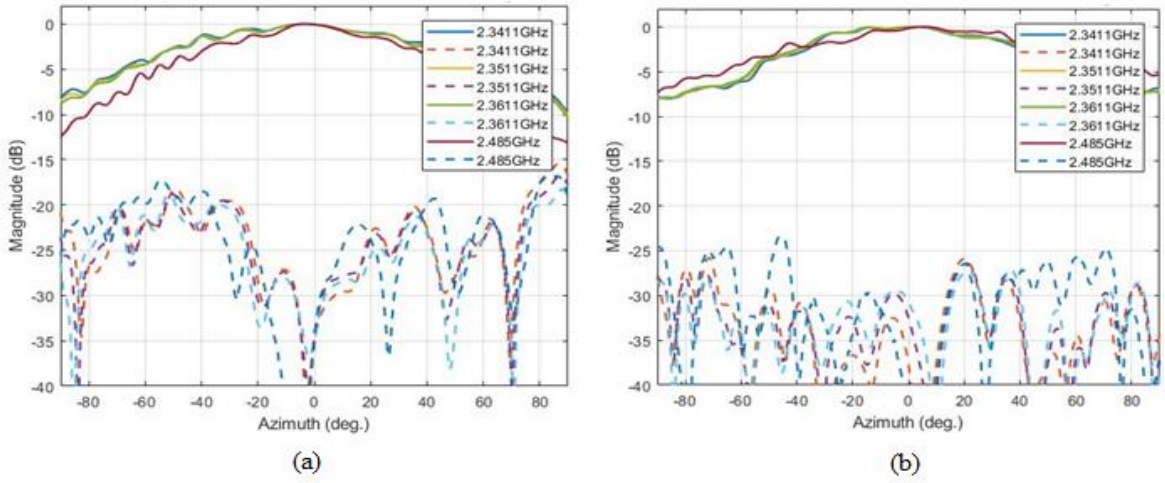

Figure 5.4.9 (a) Measured co-polar and cross-polar radiation patterns for the conventional patch antenna at ϕ=0 deg. (b) Measured co-polar and cross-polar radiation patterns for the conventional patch antenna at ϕ=90 deg.

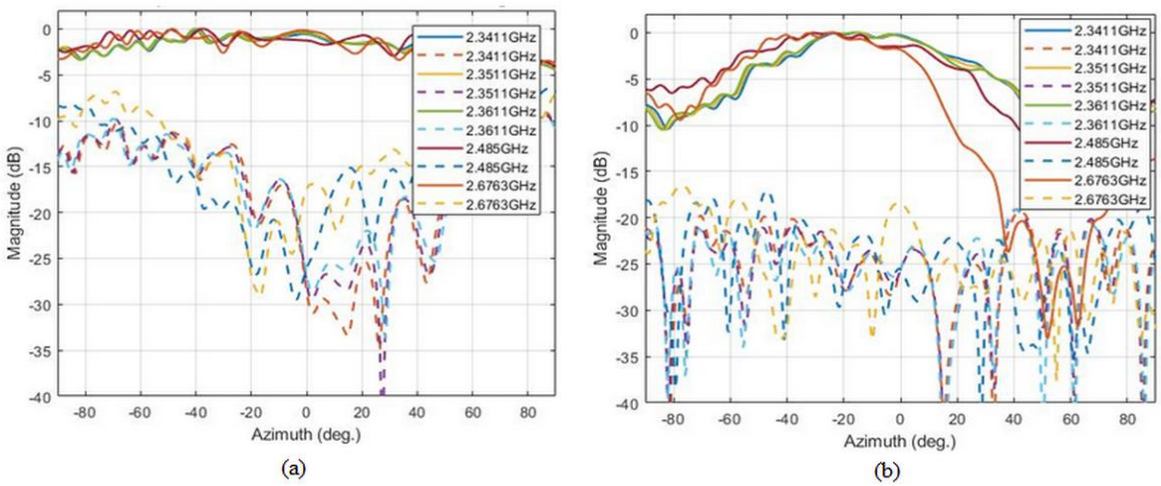

Figure 5.4.10 (a) Measured co-polar and cross-polar radiation patterns for the modified antenna at ϕ=0 deg., (b) Measured co-polar and cross-polar radiation patterns for the modified antenna at ϕ=90 deg.

Table 5.4.1 shows the comparison between the conventional patch antenna and the modified patch antenna. It shows that in addition to RCS reduction, the modified design shows improvement in Reflection Coefficient. The -10 dB impedance bandwidth is increased to 415.4 MHz. The increase in the bandwidth is attributed to the reduced quality factor. So the modified structure offers RCS reduction, improved Reflection Coefficient, gain and bandwidth enhancement.

Table 5.4.1. Comparative analysis between the conventional patch and the modified patch antenna

Sr. No.	**Parameter**	**Conventional Patch Antenna**	**Patch antenna loaded with JC structure**
1	Patch Dimensions	30.14 mm × 30.14 mm (0.24λ × 0.24λ)	16.7 mm × 16.7 mm (0.145λ × 0.145λ)
2	Reflection coefficient	-14 dB	-33 dB
3	-10 dB Imp. BW	49.6 MHz	415.4 MHz

Table 5.4.2 shows the advantages of the proposed design as compared with the published work. The comparison parameters include RCS reduction, angular stability, frequency band for RCS reduction, size reduction, gain enhancement and integration of the metasurface with patch antenna. It is observed that Metamaterial Absorbers show narrowband performance and they do not offer size reduction. The coding metasurfaces reported are not integrated with the patch antennas. Some designs do not exhibit angular stability and in some

designs with Radar Absorbing Materials pattern degradation can be observed. So, the proposed design shows good RCS reduction along with the additional advantages of improvement in performance parameters.

Table 5.4.2. Comparison of the proposed structure with similar work

Ref. and Year	Method Used	Freq. Band for RCS Reduction	Size Reduction, Gain Enhancement	Remarks
[13], 2006	Fractal Slot Microstrip Antenna	2.5 GHz-7.5 GHz	No Gain Enhancement; Gain loss of 0.69 dBi	RCS reduction was only for the wave incident at 60 deg.
[16], 2019	4-bit Coding Metasurface	15 GHz-40 GHz	No; Complex Design due to water cycle algorithm	Not integrated with patch antenna
[33], 2019	MTM Absorber	8 GHz-10 GHz	No	Not integrated with patch antenna
[34], 2013	Bandstop FSS	1-4 GHz, 6.6-20 GHz	No Size Reduction, No Gain Enhancement;	No significant RCS reduction within operating band at $\theta = 0$ deg.
[35], 2021	Metasurface Absorber	No RCS reduction reported	Used for a MIMO Antenna	8.75 GHz – 9 GHz, absorption band
Proposed Work	Jerusalem Cross slots in the ground plane	1.5 GHz-10 GHz	Size reduction of patch antenna (44.59%); Enhanced Gain, impedance BW (415.4 MHz)	RCS reduction for oblique incidence upto 70 deg.

5.5) Contribution 5: Comparison between low-RCS antennas designed using other methodologies like slotted Jerusalem Crosses and Strips and combination of CSRR and Fractals

In this section, comparison between various RCS reduction techniques is included. The comparison includes the design methodology, RCS reduction bandwidth, angular stability, antenna parameters and design complexity. It helps to evaluate the most promising methods of RCS reduction of antennas.

5.5.1) Antenna designed with slotted Jerusalem Cross and Strips in the ground plane

In this work, FSS unit cells are designed with the help of Slotted Jerusalem Crosses and Strips. Excellent RCS reduction can be obtained in C-band and X-band. The antenna parameters like gain and bandwidth are improved. The structure showed good RCS reduction for TE and TM modes. The conventional patch antenna is designed for 5.93 GHz resonant frequency on Rogers RT-Duroid 5880 substrate. The relative permittivity of the substrate is

2.2. The loss tangent of the material is 0.0009. The ground plane of the simple patch antenna is loaded with the bandstop Frequency Selective Surface. The center frequency of the structure is 6 GHz. The dimensions of the patch antenna are 15.3 mm × 21 mm. The ground plane dimensions are 64.62 mm × 64.62 mm. A 50 ohm coaxial cable is used to excite the patch antenna. The antenna design is simulated in CST Microwave Studio software. The modified antenna resonates at the frequency of 5.97 GHz. Fig. 5.5.1 (a) shows the geometry of the unit cell and Fig. 5.5.1 (b) shows the bottom view of the antenna with FSS.

The dimensions of the structure in mm are as follows. d1=21.54, d2=11.4, d3=1.8, d4=5.6, g1=1, g2=10.6, w1=0.1, w2=0.2 and w3=2.5. The length of the patch antenna is 15.3 mm and the width of the patch antenna is 21 mm. The substrate height is 1.5748 mm. The length and width of the ground plane are 64.62 mm. The dimensions of the structure are obtained through software optimization process.

The monostatic RCS values of the conventional antenna and the modified antenna are plotted in Fig. 5.5.2 for the normal incidence. JC structure and intersecting strips form a bandstop metasurface which can be used for RCS reduction.

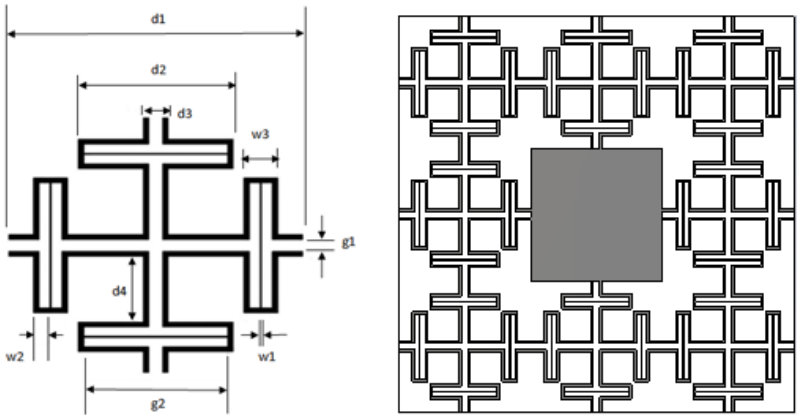

Figure 5.5.1. (a) Geometry of the bandstop FSS, (b) Bottom view of the modified antenna

The conventional patch antenna shows minimum RCS value of -18 dB at the frequency of 5.75 GHz. In the case of the modified antenna, significant RCS reduction can be obtained for the frequency range of 3-13 GHz. RCS reduction up to -55 dB can be achieved with the help of bandstop metasurface. Angular stability of the structure can also be verified by changing the angle of the incident wave. The angle of incidence is made 60 deg. and RCS values are obtained. Fig. 5.5.3 (a) shows the RCS of the modified antenna for θ=60 deg. and ϕ=0 deg. RCS value as low as -46.5 dBsm is obtained at 4 GHz.

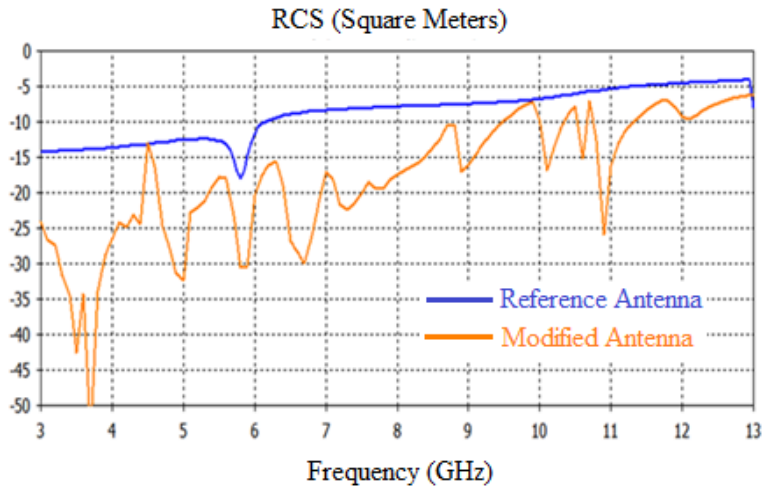

Figure 5.5.2. RCS comparison of the reference patch antenna and the modified antenna

For other frequencies overall RCS remains quite lower than that of the conventional antenna. So, overall RCS reduction is obtained for the frequency range of 3-13 GHz for this angle of incidence. Fig. 5.5.3 (b) shows the RCS of the modified antenna when the E-field is rotated by 90 deg. and θ=15 deg. RCS as low as -34 dBsm is obtained at the frequency of 3.5 GHz. The simulated results show that RCS reduction can also be obtained when the E-field is rotated by 90 deg.

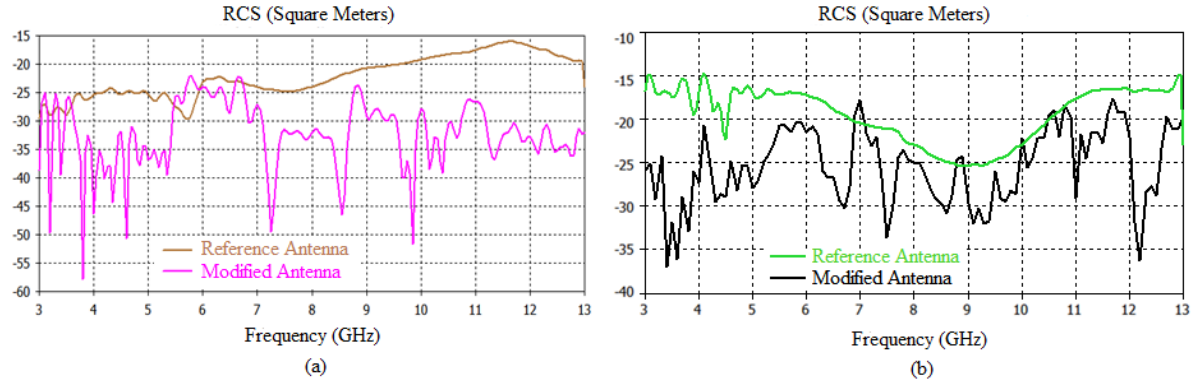

Figure 5.5.3. RCS comparison of the conventional patch antenna and the modified antenna (a) θ=60 Deg., (b) θ=15 Deg., α=90 Deg.

Fig. 5.5.4 (a) and Fig. 5.5.4 (b) show the gain patterns of the conventional antenna in the ϕ=0 Deg. plane and in the ϕ=90 Deg. plane. For the conventional antenna, the value of gain is 7.72 dB in the ϕ=0 Deg. plane and 7.67 dB in the ϕ=90 Deg. plane. Fig. 5.5.4 (c) and Fig. 5.5.4 (d) show the gain patterns of the modified antenna in the ϕ=0 Deg. plane and in the ϕ=90 Deg. plane. For the modified antenna, the value of gain is 8.12 dB in ϕ=0 Deg. plane and 8.04 dB in ϕ=90 Deg. plane.

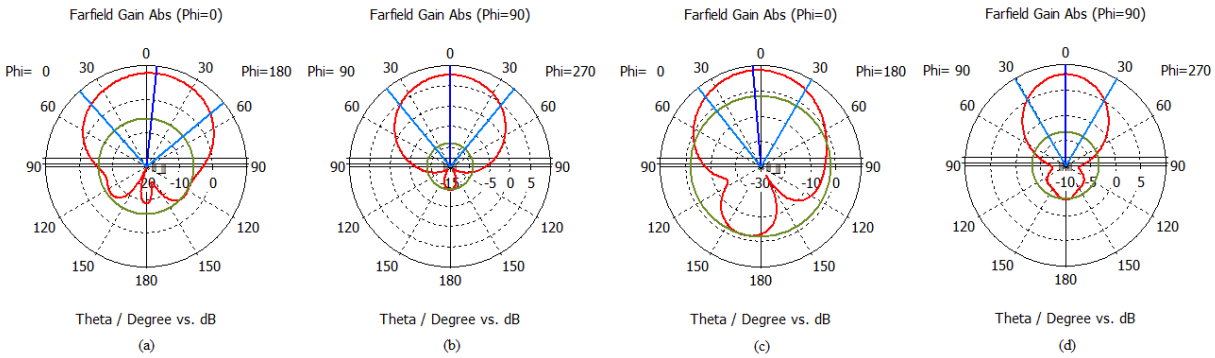

Figure. 5.5.4. Gain Patterns of the Ref. Antenna in (a) ϕ = 0 Deg. Plane, (b) ϕ = 90 Deg. Plane; Gain Patterns of the modified antenna, (c) ϕ = 0 Deg. Plane, (b) ϕ = 90 Deg. Plane.

5.5.2) Antenna designed with combination of CSRR and Fractal structures in the ground plane

In this work, the lossy property of the Complimentary Split Ring Resonator structure is improved by the Koch curves. The fractal structures are used because of their space-filling properties. The conventional rectangular patch antenna is designed on F4B-2 substrate with thickness 2 mm. The relative dielectric constant of the substrate is 2.65 and it has loss tangent of 0.0009. The antenna resonates at 3.45 GHz. The value of the Reflection Coefficient of the Reference Antenna is around -29 dB. The low-RCS antenna resonates at the frequency of 3.31 GHz and the value of reflection coefficient is around -33 dB. The antennas are simulated in CST Microwave Studio software. Fig. 5.5.1 (a) and Fig. 5.5.2 (b) show the top view and the bottom view of the modified antenna.

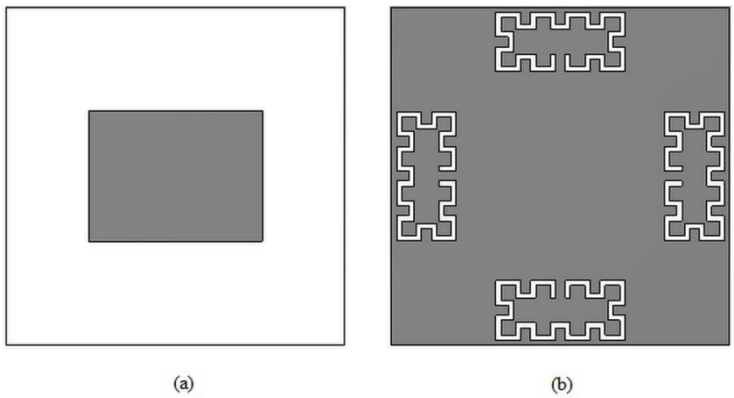

Figure 5.5.1. Antenna loaded with CSRR and fractals (a) Top view, (b) Bottom view

The fractal structures are designed on the periphery of the Complimentary Split Ring Resonator structure. The fractal structures increase the length of the slots keeping the total dimensions same. The quality factor of the circuit is given by,

$$Q = \frac{1}{R}\sqrt{\frac{L}{C}} \tag{5.5.1}$$

Since the capacitance increases, the quality factor decreases. Reduced quality factor indicates higher loss. The fractal structures increase the coupling so the lossy property is further improved. The distance of the modified CSRR structure is chosen in such a way that the radiation characteristics of the antenna do not degrade with respect to the conventional antenna. The resonant frequency of this structure is kept away from the operating band of the antenna. Figure 5.5.2 shows the structural mode monostatic Radar Cross Section of the conventional antenna and the modified antenna. In the case of Reference Antenna the minimum value of RCS is -21.6 dBsm at the frequency of 3.4 GHz. In the case of antenna with combination of CSRR and Fractals, the RCS reduction peaks are observed at the frequencies of 2.75 GHz and 3.44 GHz. The RCS values are around -40 dBsm and -27 dBsm respectively. So, good RCS reduction is observed at the resonant frequency of the modified CSRR structure.

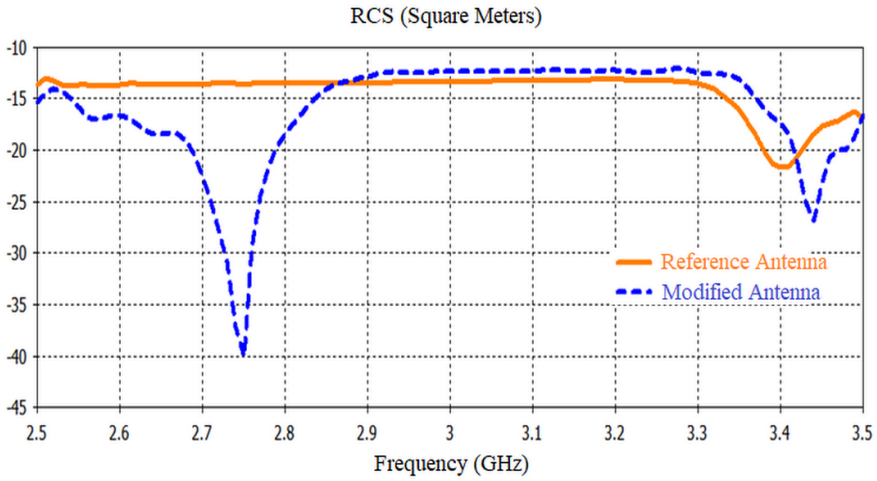

Figure 5.5.2. RCS of the Reference Antenna and the Modified Antenna

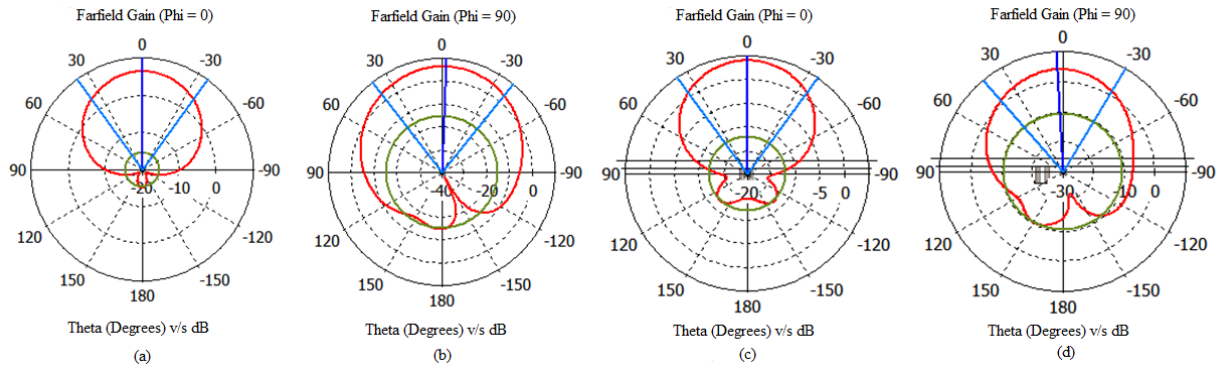

Figure 5.5.3. Gain Patterns of the Ref. Antenna in (a) ϕ = 0 Deg. Plane, (b) ϕ = 90 Deg. Plane; Gain Patterns of the modified antenna in (c) ϕ = 0 Deg. Plane, (b) ϕ = 90 Deg. Plane.

Fig. 5.5.3 shows the Gain patterns of the Reference Antenna and the Low-RCS Antenna in both the planes. The gain value of the Reference Antenna is 6.36 dB in the ϕ=0

Deg. plane and 6.38 dB in the ϕ=90 Deg. plane. The peak gain value of the Modified Antenna is 4.03 dB in the E-plane and 4.06 dB in the H-plane. Table 5.5.1 shows the comparison between various designs and methodologies. From the comparative analysis, it is apparent that the proposed antenna designs exploiting the use of Polaization Conversion Metasurface and Artificial Magnetic Conductors outperform and the objectives are achieved as per the problem definition.

Table 5.5.1 Comparison between various designs

Type of the design	**Methodology Used**	**Features**	**Per. BW**	**Design Complexity**
Proposed Design I (PCM I) (FR-4)	Polarization Converters	Excellent Angular Stability w.r.t various angles of incidence and Polarization (TE as well as TM), Out-of-band RCS reduction	Overall RCS reduction BW (3.49 – 20 GHz, 140.57% as compared with PEC), (4.22 – 11.55 GHz, 93% as compared with patch)	Coplanar Integration
Proposed Design II (PCM II) (FR-4)	Polarization Converters	Wideband RCS reduction, In-band as well as Out-of-band RCS reduction	7.2 GHz -24.8 GHz (110%)	Coplanar Integration
Proposed Design III using AMCs (FR-4)	Artificial Magnetic Conductors	Wideband RCS Reduction, Better Angular Stability, In-band as well as out-of-band RCS reduction	Overall RCS reduction BW (5.6 GHz – 24.3 GHz, 125.08% as compared with PEC), 10 dB RCS reduction BW (8.38 GHz – 16.1 GHz (63.07%)	Single Layer Design
Patch antenna with Jerusalem Cross slots (Proposed Design IV) (FR-4)	Jerusalem Cross slots	Enhanced Gain, impedance BW (415.4 MHz); Size reduction of patch antenna (44.59%), Angular stability for the wave incident from 0 deg. to 72 deg.	1-10 GHz	Planar configuration
Design with Bandstop Structure (Rogers RT-5880)	Intersecting Strips and Jerusalem Cross Slots	Significant RCS reduction for various incident angles and for TE and TM polarization	3-13 GHz (125%)	Single Layer Design
Antenna with Fractal CSRR slots (F4B2)	Fractals on the periphery of CSRR slots	Excellent RCS reduction for wide range of incident angles	2.5 GHz - 2.85 GHz (13.08%), Peak RCS reduction at 2.75 GHz	Planar Configuration

6) Conclusion

Metasurfaces are alternatives to bulk three dimensional metamaterials. They require less physical space and can exhibit lower loss. Traditional Frequency Selective Surfaces, Metasurfaces and Absorbers exhibit narrow RCS reduction bandwidth. Use of Radar Absorbing Materials degrades the Antenna Radiation Pattern. Wideband Radar Cross Section reduction can be achieved with the help of Metasurfaces like Polarization Conversion Metasurface and Artificial Magnetic Conductors. Use of Polarization Converter Metasurface gives better performance as compared with other techniques exploiting absorbers and frequency selective surfaces. Checkerboard metasurfaces, AMCs and combination of single and dual band AMCs can be used for wideband RCS reduction and better angular stability. Excellent RCS reduction can be achieved without degradation of antenna radiation pattern and other performance parameters with these techniques if proper optimization is done.

7) Future Scope

The proposed designs mainly include the use of Polarization Conversion Metasurface and Artificial Magnetic Conductors. New designs of Polarization Conversion Metasurface can be investigated to extend the RCS reduction bandwidth. Checkerboard metasurfaces involving the use of triple-band AMCs can also be designed to design low-RCS antennas if the required phase difference can be maintained. The quaternionic metasurfaces and coding metasurfaces can be developed for RCS reduction of larger structures. 3D Printed Metamaterials are also being developed for stealth applications. The modulated metasurfaces and non-periodic checkerboard surfaces also increase RCS reduction bandwidth. To minimize the time-consuming simulations the techniques of Particle Swarm Optimization are also being investigated to design Low-RCS antennas.

The research work deals with RCS reduction of a single patch antenna. But the designs based on Polarization Conversion Metasurface and Artificial Magnetic Conductors have potential applications in the field of stealth technology. So, the proposed concepts can also be extended to patch antenna arrays.

8. PUBLICATIONS

➢ Research Papers published in International Journals

1. Krunal Patel, Dr. M. Joshi, "Wideband Radar Cross Section Reduction of Microstrip Patch Antenna using Polarization Converter Metasurface," Defence Science Journal, Vol. 72, No. 4, pp. 568-580, Aug. 2022.
   doi: 10.14429/dsj.72.17818.
   (Indexed in Scopus, Web of Science, SCIExpanded etc., IF: 0.7)
2. Krunal Patel, Dr. M. Joshi, "Broadband Radar Cross Section Reduction of Microstrip Antenna Using Polarization Conversion Metasurface," Progress In Electromagnetics Research B, Vol. 96, pp. 67-86, 2022.
   doi: 10.2528/PIERB22060405
   (Indexed in Scopus, Compendex, CrossRef etc.)
3. K. Patel, M. Joshi, "Wideband RCS reduction of microstrip antenna using artificial magnetic conductor metasurface," Springer SADHANA, vol. 48, no. 88, 2023.
   (Indexed in Scopus, Web of Science, SCIExpanded, ProQuest etc., IF: 1.6)
   doi: 10.1007/s12046-023-02141-z
4. Krunal Patel, Dr. M. Joshi, "Metamaterials and metasurfaces : Contemporary Approaches in Antenna Design," International Journal of Research in Electronics and Computer Engineering, Volume 7, Issue 2, pp. 769-778, 2019.
   (UGC Approved)

➢ Research Papers published/presented in International Conferences

1. Krunal Patel, Dr. M. Joshi, "Radar Cross Section Reduction of Microstrip Patch Antenna using Metasurface," AIP Conference Proceedings, vol. 2717, no. 1, June 2023, pp. 060001-060013.
   doi: 10.1063/5.0129260
   (Indexed in Scopus, Web of Science etc.)
2. Krunal Patel, Dr. M. Joshi, "Size and RCS Reduction of Microstrip Patch Antenna using Jerusalem Cross Structure," Presented at the 13th Annual International Conference of Antenna Test and Measurement Society (ATMS) of India, 2021.

9) References:

1. K. Konstantinidis, A. P. Feresidis and P. S. Hall, "Broadband Sub-Wavelength Profile High-Gain Antennas Based on Multi-Layer Metasurfaces," *IEEE Transactions on Antennas and Propagation*, vol. 63, no. 1, pp. 423-427, Jan. 2015.
2. L. Chen, Z. Lei, R. Yang, J. Fan and X. Shi, "A Broadband Artificial Material for Gain Enhancement of Antipodal Tapered Slot Antenna," *IEEE Transactions on Antennas and Propagation*, vol. 63, no. 1, pp. 395-400, Jan. 2015.
3. Hao Y. W., Liu Y., Li. K. et al., "Wideband radar cross-section reduction of microstrip patch antenna with split-ring resonators," *Electronic Letters*, vol. 51, no. 20, pp. 1608-1609, 2015.
4. Liu, X., Gao, J., Cao, X. Y. et al., "A high gain and low scattering waveguide slot antenna of artificial magnetic conductor octagonal ring arrangement," *Radioengineering*, vol. 25, no. 1, pp. 46-52, 2016.
5. Hu Tao, Nathan I. Landy, Christopher M. Bingham, Xin Zhang, Richard D. Averitt, and Willie J. Padilla, "A metamaterial absorber for the terahertz regime: Design, fabrication and characterization," *Opt. Express*, vol. 16, pp. 7181-7188, 2008.
6. Hui Li, Li Hua Yuan, Bin Zhou, Xiao Peng Shen, Qiang Cheng, and Tie Jun Cui, "Ultrathin Multiband gigahertz metamaterial absorbers," *Journal of Applied Physics*, vol. 110, 014909, 2011.
7. Nguyen, T.T. and S. Lim, "Angle and polarization insensitive broadband metamaterial absorber using resistive fan –shaped resonators," *Applied Physics Letters*, vol. 112, No. 2, 021605, 2018.
8. F. Yuan et al., "Broadband RCS reduction based on spiral-coded metasurface," *IEEE Antennas Wireless Propag. Lett.*, vol. 16, pp. 3188-3191, Nov. 2017.
9. Li SJ, Gao J, Cao XY, Zhao Y, Zhang Z, Liu HX, "Loading metamaterial perfect absorber method for in-band radar cross section reduction based on the surface current distribution of array antennas," *IET Microwaves, Antennas & Propagation*, vol. 9, no. 5, pp. 399-406, 2015.
10. S. Genovesi, F. Costa, A. Monorchio, "Wideband radar cross section reduction of slot antennas arrays," *IEEE Trans. Antennas Propagat.*, vol. 62, no. 1, pp. 163-173, Jan. 2014.
11. Ding F, Cui Y, Ge X, Jin Y, He S., "Ultra-broadband microwave metamaterial absorber," *Applied Physics Letters*, vol. 100, 103506, 2012.

12. Chen H., Zhou P., Chen L., Deng L., “Study on the properties of surface waves in coated RAM layers and monostatic RCS performances of the coated slab,” *Progress in Electromagnetics Research M*, vol. 1, pp. 123-135, 2010.
13. Liu, Y., X.-G. Shu, and B.-Z. Hong, “A novel fractal slot microstrip antenna with low RCS,” *2006 IEEE AP-S International Symposium on Antennas and Propagation and USNC/URSI National Radio Science Meeting*, Albuquerque, New Mexico, USA, 2006, pp. 2603–2606.
14. Q. Gao, Y. Yin, D. B. Yan, and N. C. Yuan, “Application of metamaterials to ultra- thin radar absorbing materials design,” *Electron. Lett.*, vol. 41, no. 17, pp. 936–937, 2005.
15. Li-Na Chen, Yong-Chang Jiao, Huan-Huan Xie, Fu-Shun Zhang, “Minkowski fractal patch antenna for size and radar cross section reduction,” *Proceedings of 2011 IEEE CIE International Conference on Radar*, Chengdu, China, 2011, pp. 1406-1409.
16. Fuheng Zhang, Feng Xu, Guo-Min Yang, A.B. Waqas, “4-bit optimized coding metasurface for wideband RCS reduction,” *IEEE Access*, vol. 7, pp. 122378-122386, August 2019.
17. Pouyanfar, N., Nourinia, J. & Ghobadi, C, “Multiband and multifunctional polarization converter using an asymmetric metasurface,” *Sci. Rep*., vol. 11, 9306, 2021.
18. Jafari, F.S., Naderi, M., Hatami, A., Zarrabi, F.B., “Microwave Jerusalem Cross absorber by metamaterial split ring resonator load to obtain polarization independence with triple band application,” *AEU- International Journal of Electronics and Communications*, vol. 101, pp. 138-144, 2019.
19. Wang, S., Chen, M., Wang, J., Zhang, Z., Li, Z. & Li, Y, “Radar cross section reduction of a microstrip antenna with CSRRs loaded on the ground,” *in 11th International Symposium on Antennas, Propagation and EM Theory (ISAPE)*, Guilin, China, 2016, pp. 670-673.
20. Yang, D., Lin, H. & Huang, X., “Dual Broadband Metamaterial Polarization Converter in microwave regime,” *Prog. Electromagn. Res. Lett*., vol. 61, pp. 71-76, 2016.
21. Feng, M.; Wang, J.; Ma, H.; Mo, W.; Ye, H.; Qu, S., “Broadband polarization rotator based on multi-order plasmon resonances and high impedance surfaces,” *J. Appl. Phys*., vol. 114, 074508, 2013.
22. Zhang X.L., Niu M., Su L.H. and Song K.P., “Radar Cross Section Reduction Based on Metasurface,” In: Li B., Shu L., Zeng D. (eds) Communications and Networking. ChinaCom 2017. *Lecture Notes of the Institute for Computer Sciences, Social Informatics and Telecommunications Engineering*, 236. Springer, Cham, 2018.

23. Li Jianxing, Khan Tayyab Ali, Meng Xianjia, Chen Juan, Peng Gantao and Zhang Anxue, “Wideband radar cross-section reduction of microstrip patch antenna using coding metasurface,” *IET Microwaves, Antennas and Propagation*, vol. 13, no. 10, pp. 1719-1725, 2019.
24. H. Ahmadi, M. J., Nayyeri, V., Soleimani, M. et al., “Pixelated Checkerboard Metasurface for Ultra-Wideband Radar Cross Section Reduction,” *Scientific Reports*, vol. 7, 11437, 2017.
25. Y. Liu, Y. Hao, K. Li and S. Gong., “Radar Cross Section Reduction of a Microstrip Antenna Based on Polarization Conversion Metamaterial,” *IEEE Antennas and Wireless Propagation Letters*, vol. 15, pp. 80-83, 2016.
26. Dong Yang, Hai Lin and Xiaojun Huang, “Dual Broadband Metamaterial Polarization Converter in Microwave Regime,” *Progress In Electromagnetics Research Letters*, vol. 61, pp. 71-76, 2016.
27. F. Samadi and A. Sebak, "Dielectric Based Triangle-type AMC Structure for RCS Reduction at Mmwave Frequencies," *2020 IEEE International Symposium on Antennas and Propagation and North American Radio Science Meeting*, 2020, pp. 1193-1194.
28. Huicun Yu, Xiangyu Cao, Jun Gao, Huanhuan Yang, Liaori Jidi, Jiangfeng Han, and Tong Li, “Design of a wideband and reconfigurable polarization converter using a manipulable metasurface,” *Opt. Mater. Express*, vol. 8, pp. 3373-3381, 2018.
29. X. Liu, J. Gao, L. Xu, X. Cao, Y. Zhao and S. Li, “A Coding Diffuse Metasurface for RCS Reduction,” *IEEE Antennas and Wireless Propagation Letters*, vol. 16, pp. 724-727, 2017.
30. Zheng Yue-Jun, Jun Gao, Xiang-yu Cao, Si-jia Li, Wen qiang Li, “Wideband RCS reduction and gain enhancement microstrip antenna using chessboard configuration superstrate,” *Microwave and Optical Technology Letters*, vol. 57, no. 7, pp. 1738-1741, July 2015.
31. Babar Kamal, Jingdong Chen, Ying Yingzeng, Jian Ren, Sadiq Ullah, and Wasi Ur Rehman Khan, “High efficiency and ultra-wideband polarization converter based on an L-shaped metasurface,” *Opt. Mater. Express*, vol. 11, pp. 1343-1352, 2021.
32. Z. Liu, Y. Liu and S. Gong, “Gain Enhanced Circularly Polarized Antenna With RCS Reduction Based on Metasurface,” *IEEE Access*, vol. 6, pp. 46856-46862, 2018.
33. S. Chejarla, S.R. Thummaluru, “Flexible metamaterial absorber with wide incident angle insensitivity for conformal applications,” *Electronic Letters*, vol. 55, no. 3, pp. 133-134, February 2019.

34. S. Chejarla, S.R. Thummaluru, “Flexible metamaterial absorber with wide incident angle insensitivity for conformal applications,” *Electronic Letters*, vol. 55, no. 3, pp. 133-134, February 2019.
35. G. Saxena, Y.K. Awasthi, Priyanka Jain, “Design of metasurface absorber for low RCS and high isolation MIMO antenna for radio location & navigation,” *AEU - International Journal of Electronics and Communications*, vol. 133, 153680, 2021.